Two-Phase Flow in the Microvasculature

Talfan Evans

Keble College, Oxford

Supervisor: Dr. Stephen J. Payne

Trinity 2013

FINAL HONOUR SCHOOL OF ENGINEERING SCIENCE
DECLARATION OF AUTHORSHIP

You should complete this certificate. It should be bound into your fourth year project report, immediately after the title page. **Three copies** of the report should be submitted to the Chairman of Examiners for the Honour School of Engineering Science, c/o Clerk of the Schools, Examination Schools, High Street, Oxford.

Name (in capitals): SION TALFAN EVANS

College (in capitals): KEBLE **Supervisor: DR. STEPHEN J. PAYNE**

Title of project (in capitals): TWO-PHASE FLOW IN THE MICROVASCULATURE

Page count (excluding risk and COSHH assessments): 50

Please tick to confirm the following:

I have read and understood the University's disciplinary regulations concerning conduct in examinations and, in particular, the regulations on plagiarism (*Essential Information for Students. The Proctors' and Assessor's Memorandum*, Section 9.6; also available at www.admin.ox.ac.uk/proctors/info/pam/section9.shtml).	☐
I have read and understood the Education Committee's information and guidance on academic good practice and plagiarism at http://www.ox.ac.uk/students/academic/goodpractice/ .	☐
The project report I am submitting is entirely my own work except where otherwise indicated.	☐
It has not been submitted, either partially or in full, for another Honour School or qualification of this University (except where the Special Regulations for the subject permit this), or for a qualification at any other institution.	☐
I have clearly indicated the presence of all material I have quoted from other sources, including any diagrams, charts, tables or graphs.	☐
I have clearly indicated the presence of all paraphrased material with appropriate references.	☐
I have acknowledged appropriately any assistance I have received in addition to that provided by my supervisor.	☐
I have not copied from the work of any other candidate.	☐
I have not used the services of any agency providing specimen, model or ghostwritten work in the preparation of this thesis/dissertation/extended essay/assignment/project/other submitted work. (See also section 2.4 of Statute XI on University Discipline under which members of the University are prohibited from providing material of this nature for candidates in examinations at this University or elsewhere: http://www.admin.ox.ac.uk/statutes/352-051a.shtml#_Toc28142348.)	☐

The project report (excluding risk and COSHH assessments) does not exceed 50 pages (including all diagrams, photographs, references and appendices).	☐
I agree to retain an electronic copy of this work until the publication of my final examination result, except where submission in hand-written format is permitted.	☐
I agree to make any such electronic copy available to the examiners should it be necessary to confirm my word count or to check for plagiarism.	☐

Candidate's signature: …… Date: ..……..

Department of Engineering Science

Risk Assessment

Risk Assessment of:	Models of Two Phase Flow in the Microvasculature				Page:	1/1
In Building:	Thom Building / IBME / Keble College			Review Date :		
Assessment Undertaken by:	Talfan Evans	Signed:		Date :	21/11/12	
Assessment Supervisor:	Dr. Stephen J. Payne	Signed:		Date :	21/11/12	

Hazard	Persons at Risk	Risk Controls In Place	Further Action Necessary To Control Risk
Back Pain.	Author.	Take Regular Breaks. Adopt correct posture (Forearms parallel to the desk). Adjust seating height.	Use seating with appropriate lumbar support. Refer further issues to GP.
Neck Pain.	Author.	Take regular breaks. Adjust screen height (Eyes level with top of screen).	Refer further issues to GP.
Eye strain.	Author.	Take regular breaks. Reduce screen brightness. Ensure adequate lighting.	Refer further issues to GP / Optician.
Leg ache.	Author.	Take regular breaks for light exercise. Ensure adequate space beneath desk.	Refer further issues to GP.
Electrical Shock.	Author.	Ensure that no liquids or foods be consumed near computer. Maintain integrity of electronic parts (power adapters, electrical connections).	Replace damaged electrical parts.

Contents

Acknowledgements

A great deal of thanks is owed to Dr. Stephen Payne for his support in producing this document. His advice and guidance has been invaluable, and has helped to inspire a genuine interest in the work.

Abstract

The present study attempts to model the separation of blood flows occurring in mammalian blood vessels of diameters between 50-300μm. Two mathematical models are proposed to explain this two-phase flow, which consists of a red blood cell rich core layer surrounded by a cell depleted plasma layer. The first attempts to predict the radius at which the phase separation boundary occurs through the minimisation of shear energy dissipation, in the case of various fluid models. It is found that there does exist a boundary position for which shear energy is minimised, but that the values are not in good agreement with experimental data. The second investigates migration of cells due to both lift effects, caused by velocity gradient induced shear forces, and a diffusive force acting in conjunction. This lift-diffusion model is shown to reproduce complex particle distributions observed experimentally, but does not predict accurately the position of the phase boundary.

1 Introduction

The efficient circulation of blood is crucial to maintaining the healthy functioning of the body. Nutrients are efficiently delivered and waste products removed from every cell, demanding a complex transportation system. This system can be functionally represented by a pump, the heart, generating a pressure that drives flow into a network of blood vessels, on a micro and macroscopic scale. Blood leaves the heart through the aorta, approximately three centimeters in diameter, and undergoes successive diminishing bifurcations ending in the micrometer scale capillaries. These exist in close proximity to the cells, where nutrients essential to important metabolic processes are delivered, and harmful waste products removed by diffusion and bulk transfer through cellular pores. Capillaries are ideally adapted to facilitating this nutrient exchange, consisting of a single cell thick endothelial layer which minimises the diffusion distance whilst maximising the available surface area. Each vessel in the vascular tree is similarly suited to performing its specific function, which varies greatly according to the scale of transport. Connecting the primary arteries to the capillaries are the arterioles, regarded as the resistance vessels of the vascular system. Consisting mainly of smooth muscle, arterioles constrict or dilate according to neural and hormonal signals, causing a change in hydrostatic pressure in the capillaries and controlling the rate of

exchange, enabling the cardiovascular system to respond effectively to metabolic demand.

The field of haemodynamics studies the mechanics of blood transport, and is essential to the advancement of clinical devices and treatment. The importance of haemodynamic research is evident in the ever increasing number of those affected by cardiovascular diseases today, due in part to an aging population fed on increasingly calorific diets. Flow in the larger vessels has been studied in great detail and is considered to be well understood, with its behaviour being easily observable. Macroscopic models of blood characterised by high Reynolds numbers are not however applicable within the microvasculature, normally taken to refer to to vessels of less than 300μm in diameter, where viscous forces dominate inertial effects. These low Reynolds numbers in combination with the multi-constituent nature of blood produce complex behaviour, research into which has been historically limited by the difficulty of examining behaviour on such small length scales.

It is important to note that the large scale characteristics of haemodynamic systems are ultimately governed by their behaviour at microscopic scales. Furthermore, modern advances in surgical techniques and stenting technology mean that intervention in cases of blood clots and other adverse conditions occur on an increasingly small scale, and so it is imperative that the blood flows in these instances be fully understood.

There are three principal effects, observed exclusively in the microvasculature, that are of particular interest to this investigation. In reference to the first, the 'Fåhraeus–Lindqvist Effect' [1], Pries et al. [2] state that "it has been known for a long time that blood viscosity depends not only on haematocrit, plasma protein concentration, and temperature but also on the shear forces applied". This effect describes the significant decrease in apparent viscosity observed both *in vivo* and *in vitro*, in vessels of 50-300μm [1] in diameter, generally attributed to the high shear rates present when erythrocyte diameters become comparable to those of the conduit. Secondly, this has been linked to the occurence of two-phase flows in microvessels, where both a red blood cell rich core and cell-free peripheral plasma layer are observed. Thirdly, the Segré-Silberberg effect [3] describes the formation of an annulus of red blood cells around the centre of the vessel, with cell-free plasma in the periphery of the vessel and a core of reduced cell density.

Whilst some research has been done into these effects, they are not currently well understood, due largely to the complexity of dealing with multiple fluid phases and discreet suspended particulates. These systems are often not amenable to analytical approaches, and instead require numerical approaches that may not have been available at the time of their discovery. This investigation will thus examine

the behaviour of blood in these vessels, with particular attention to the effects of two-phase flow. Two mathematical models are proposed to predict the position of the two-phase boundary based on different physical considerations, as discussed in the following chapters. Furthermore, the effects of this boundary layer on the characteristics of the flow will be analyzed, and their physiological basis examined.

2 Literature Review

2.1 Background Physiology

Blood is a complex fluid, consisting of two major components. The first is the plasma, typically occupying 52-62% [4] by volume; this in turn consists of approximately 91.5% water, 7% proteins and the remainder of white blood cells (leucocytes), platelets (thrombocytes) and dissolved nutrients. The leucocytes act as an immune barrier, attacking foreign materials, whereas the thrombocytes act to coagulate blood, preventing losses in open wounds. The proteins provide numerous functions, balancing the osmotic blood pressure and helping to bind thrombocytes during coagulation.

The second component is that of the red blood cells, known as erythrocytes, comprising the remaining fraction of the volume, known as the haematocrit. The erythrocyte's main function is to bind oxygen molecules for transport, for which purpose it has developed a specialized biconcave shape of typically 6-8μm in diameter, which both maximizes its surface area for efficient exchange, and reduces the atherogenic buildup of fatty deposits through promoting laminar flow [5]. If the erythrocytes are deformed as in the case of sickle-cell disease, tissue damage and coagulation occurs, which emphasizes the advantage of their adapted form.

2.2 Rheological Models of Blood

Rheology is the study of the deformation and flow of matter. Of the numerous models developed to describe fluid flows, the ones most relevant to blood flow are discussed in the following sections.

2.2.1 Power-Law Fluids

The power-law fluids are a group of fluids whose shear stress τ is taken to vary according to the expression:

$$\tau = K\left(\frac{\partial u}{\partial r}\right)^n = \left[K\left(\frac{\partial u}{\partial r}\right)^{n-1}\right]\left(\frac{\partial u}{\partial r}\right) = \eta_{eff}\left(\frac{\partial u}{\partial r}\right) \tag{1}$$

where $K\,(Pa.s^n)$ is the flow consistency index, n the dimensionless flow behaviour index, η_{eff} the effective viscosity, u the axial velocity and $\frac{\partial u}{\partial r}$ the radial velocity gradient. It is clear that a Newtonian fluid

is simply a generalised case of a power-law fluid where the flow consistency index $n = 1$, resulting in $\eta_{eff} = \eta$. The physical representation of K can be considered as an equivalent viscosity, and n the bluntness of the flow referring to the curvature of the velocity distribution across the vessel.

Fluids with a flow behaviour index $n < 1$ are classed as pseudo-plastics, or shear-thinning fluids, so called as their effective viscosities decrease with higher shear rates. The pseudo-plastic model can be used to describe many common fluids such as paint, glycerine and other solutions of large, polymeric molecules. The behaviour of pseudo-plastics is attributed to these large molecules, which may initially be disorganized but which align themselves in the direction of an applied shear force and flow more easily, thereby reducing the effective viscosity as suggested by Reinke et al. [6].

Fluid with a flow behaviour index $n > 1$ are classed as dilatant fluids. Somewhat less common than pseudo-plastics, dilatants are characterised by their shear-thickening behaviour. As the applied shear rates increase, the effective viscosity of these fluids increases, with the mechanisms describing such behaviour being somewhat more complex.

There is evidence [7] however to suggest that blood may be classified as either of these fluid types, depending on the physical conditions under which it is observed.

2.2.2 Yield-Stress Fluids

Developing further on the power-law fluids, the Herschel-Bulkley [8] model describes another family of non-Newtonian fluids, with the introduction of the concept of a yield shear stress τ_y, an important additional aspect of the non-linear behaviour of blood. This shear dependent behaviour is compared with theat of the power-law fluids in Fig. 2, and behaves according to the following expression:

$$\tau = \tau_y + K \left(\frac{\partial u}{\partial r} \right)^n \tag{2}$$

where K and n are again the flow consistency and behaviour indices. As described by Merrill et al. [9], when the applied shear stress is less than the yield value, “only elastic strain will ensue”. However, when the shear stress exceeds that of the yield limit, “continuous viscous flow will occur”. The yield-stress can be seen therefore to correspond to the transition between

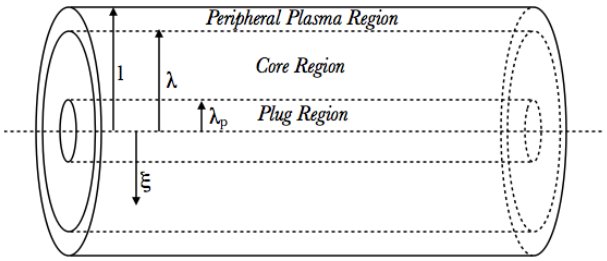

Figure 1: Three-phase flow.

elastic deformation and viscous flow. An interesting consequence of this yield-stress is that a 'plug-flow' region is predicted at the centre of the vessel, where the shear forces are lower than that of the yield limit.

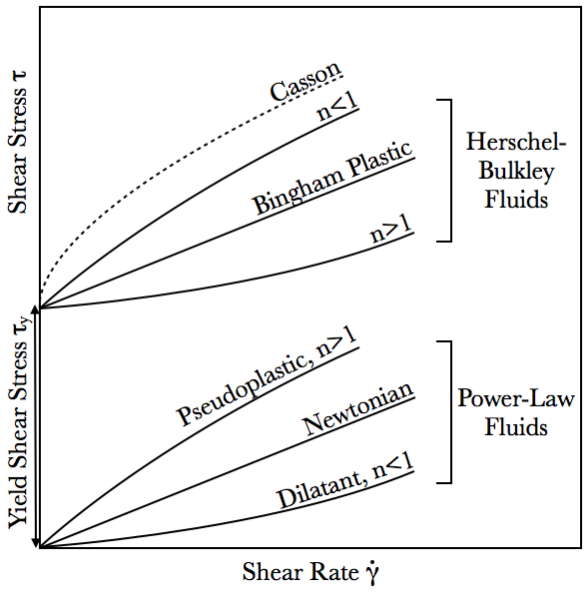

Figure 2: Shear stress vs. shear rate for the yield-stress and power-law fluids.

As described by Merill et al., within this region there will be no velocity gradient and the fluid flows as a solid plug. This will effectively result in a three-phase flow, as shown in Fig. 1. The physical origins of this behaviour are generally attributed to attractive forces existing between the suspended particulates. These forces must behave in such a way so as to permit rapid meshing of particles in stagnant flow, but be weak enough so as to decompose reversibly upon the application of sufficient shear stress. These inter-particle forces have been attributed at the molecular level to "hydrogen bonds, electrostatic charge or in some cases simply Van der Waals fields" [9], although in the case of high molecular weight erythrocytes there may be alternative sources, based on geometrical arguments.

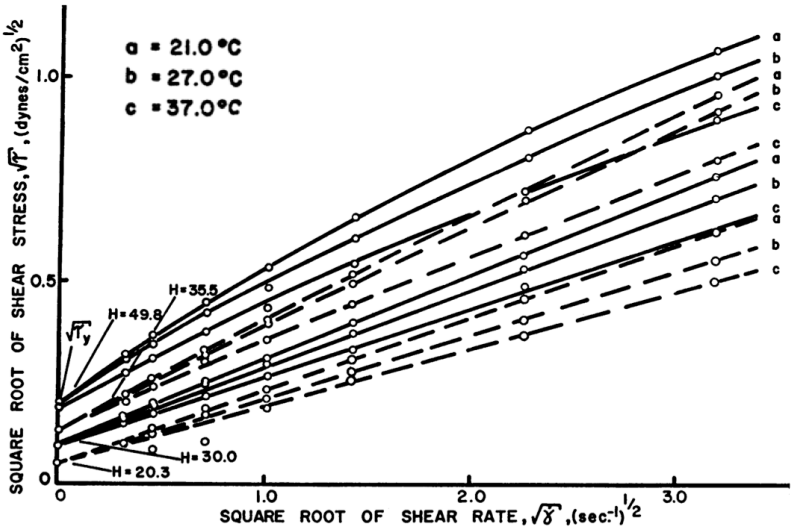

Figure 3: Casson model fitted against experimental data from Merrill et al. for a range of temperatures and tube haematocrits.

Similarly to the general Herschel-Bulkley family of fluids, the Casson [10] model also encompasses the concept of a yield-stress τ_y within the fluid, and has earned wide acceptance as a model for blood flow in microvessels. First introduced in 1959, the model was developed to describe the complex behaviour of pigment-oil suspensions in printing ink, but has since found wider applications in the modelling of paints, fats, chocolate, oil and blood dispersions. The success of the model lies in accurately describing the shear-dependent behaviour of such systems. As can be seen in Fig. 2. The Casson model belongs to the pseudo-plastic yield-stress family, but behaves slightly differently to the equivalent Herschel-Bulkley fluid, with its shear behaviour being

expressed by the equation:

$$\sqrt{\tau} = \sqrt{\tau_y} + K\sqrt{\frac{\partial u}{\partial r}} \tag{3}$$

Attempts to model blood according to the Casson equation have produced promising results. When investigating the effects of haematocrit on flow in the microvasculature, Bugliarello and Sevilla [11] compared the Casson model to their experimental data and noted that, with reference to their experiments in 40μm diameter glass tubes, the velocity distributions tend to "approach (those) of the two-fluid (Casson) model", in cases where the peripheral layer is "relatively larger". Merrill et al. [9] also commented on their findings. With regards to Fig. 3 they state that "it is evident that the Casson equation perfectly fits the data on blood at haematocrit levels of 20% and 30%". However, it should be noted that the equation is not universally applicable to all vessel radii, and that the experiments concern blood flows in small vessels at low flow rates, where the shear-dependent behaviour of blood is most clearly shown.

2.3 Two-Phase Model

Two-phase flow models have been observed and studied in a multitude of contexts. Their effects have been extensively investigated in automotive and thermodynamic conditions, in the context of air-fuel injection systems and liquid-vapour film heat transfer. By definition, two-phase flow describes the interaction of two separated phases of matter, distinguishable by individual sets of physical properties, typically studied in transport. Indeed, the hydrodynamic forces resulting from fluid flows are important in determining their defining characteristics, and form the basis of many physical theories which attempt to describe the often complex behaviour observed.

In addition to the more familiar instances of two-phase flows in engineering, recent research has concerned their importance in biomedical applications, with the effect being readily observed in the microvasculature. However, it is the nature of the two phases, specifically that of a suspended core of erythrocytes in plasma that separates this investigation from the work conducted in other engineering contexts. The particle interactions in flows of suspensions introduce additional complexity to fluid modelling, and warrant a distinct field of study. Consequently, much effort has been made to describe the aggregate behaviour of blood often in terms of 'effective' properties, through both theoretical and empirical methods, starting notably with Einstein's work [12] on dilute particle suspensions more than a hundred years ago.

A multi-phase model of blood has been adopted by many to interpret the complex behaviour observed in microvascular flows, with varying degrees of success. Recently, Sharan and Popel [13] considered a two-phase model, assuming in their analysis the fluid in both the cell-rich core and plasma peripheral

layer to behave as Newtonian fluids. They used experimental data to develop three principal equations, the first relating the ratio of tube to discharge haematocrit, developing the empirical relationship obtained by Pries et. al [2]. The tube haematocrit is a static measure of overall vessel haematocrit, considering an instantaneous cross-section of flow, whereas the discharge haematocrit accounts for the velocity distribution within the flow, and is a more useful physical measure with respect to the mass transport of blood components. The two are defined as:

$$H_T = \frac{2}{R^2}\int_0^R h\left(r\right) r dr \qquad and \qquad H_D = \frac{2}{\overline{u}R^2}\int_0^R h\left(r\right) u\left(r\right) r dr \tag{4}$$

where $\overline{u}$ is the average velocity across the vessel. In their paper, Sharan and Popel find the ratio $\frac{H_T}{H_D}$ to be constant at larger vessel diameters, but to decrease markedly at diameters less than approximately 300μm, signifying a departure from homogeneous flow to a two-phase configuration. In such a case, the cell-rich core would move faster than the peripheral plasma layer due to the decrease in shear at the centre of the vessel away from the wall, and so the tube haematocrit would appear to decrease whilst maintaining a constant mass flow rate of erythrocytes. This ratio is also demonstrated to decrease with decreasing H_T, for a constant vessel radius, according to:

$$\frac{H_D}{H_T} = H_D + \left(1 - H_D\right)\left(1 + 0.3871e^{-0.1779D} - 0.603e^{-0.0111D} - 0.0187e^{-9.06*10^{-11}D}\right) \tag{5}$$

Along with this, they also obtained from their data an expression for the apparent blood viscosity, and introduced a ratio of core-to-plasma viscosity to further develop their model. However, they found that their model was overdetermined, with three equations and two variables in haematocrit and vessel diameter. To overcome this, they introduced a plasma viscosity scaling factor intended to simulate the effects of wall friction. This is investigated further in their paper, where a numerical model is introduced based on geometric interactions between the cell and cell wall. The model shows preliminary agreement with their previous results, but is is conceded that the analysis should not be regarded as rigorous, and a more detailed study would be necessary to assess its validity.

With this system of equations they are then able to predict values of λ, the dimensionless radial position of the phase boundary, as functions of both discharge haematocrit and vessel diameter. The results compare well with experimental data obtained by Bugliarello and Sevilla [11] and Reinke et al. [6], exhibiting the correct behavioural trends although with slight differences in exact λ values. Their model predicts

the thickness of the core layer λ to increase with increasing diameter and haematocrit, agreeing with experimental observations.

Whilst the model developed by Sharan and Popel does provide accurate estimations of the core layer thickness, it is important to note that their approach is not completely deterministic, and relies on an empirical relation given by Pries et al. [2] to describe the reduction in apparent viscosity at small diameters, known as the Fåhraeus–Lindqvist effect. They also do not propose a mechanism that causes the two-phase arrangement.

Payne [14] develops further on the work done by Sharan and Popel, using a probabilistic approach based on entropy maximization following work by Chiu [15] to predict the flow behaviour in both phases. Payne demonstrated that by allowing the fluid in the plasma layer to behave according to a power-law of varying exponent, it is possible to discard the effective plasma viscosity ratio introduced by Sharan and Popel, although it is conceded that "it is possible that a combination of the two models may yield better solutions than either on its own". Through comparison with experimental data, Payne is able to determine the velocity exponent and produce velocity profiles that are in better agreement with experimental data than those predicted by the previous authors.

Bugliarello and Sevilla [11], like Sharan and Popel, consider a two-fluid model to compare with their data, but assume the fluid in the plasma layer to behave according to the Casson model [10]. They observe in great detail blood flow in glass tubes between diameters of 40-83μm in both steady and pulsatile conditions, recording accurate measurements of λ along with the radial velocity distributions for varying haematocrit and flow rates, making their data a valuable resource for many authors, including Sharan and Popel.

A comparison of results predicted by Sharan and Popel with data from Bugliarello and Sevilla and Reinke et al. is shown in Fig. 4. Like Sharan and Popel, they also find the proportional core layer thickness λ to decrease with diminishing diameter, and further note that its dimensions are not significantly altered with pressure gradient. They also observe that the blood flow tends to adhere to the two-fluid model under these conditions, as opposed to the Newtonian behaviour observed at large flow rates in large vessels. Bugliarello and Sevilla were the first to collect such detailed data on pulsatile flow in the microvasculature. Much of the existing research to date, including that of Womersley [16] had been done in larger vessels, where the multi-phasic nature of blood can largely be neglected.

From their comparisons, Bugliarello and Sevilla draw the conclusion that the typical positions of λ are "not appreciably influenced by the pulsating frequency, indeed they state that they are "essentially" the same

for both steady and pulsatile flow. Additionally, they note that the pulsatile velocity profiles are in phase with those in steady flow, and that the average pressure drops are also identical. These observations are also in good agreement with data obtained by McComis et al. [17] and Hershey and Song [18].

For the purpose of this investigation, the pulsatile aspects of blood flow are therefore not considered, as its ultimate aim is simply to produce a model capable of predicting the dimensions of λ. This is not however to state that pulsatile flow has no significant effect on other properties of flow, only that these properties are not of specific interest here.

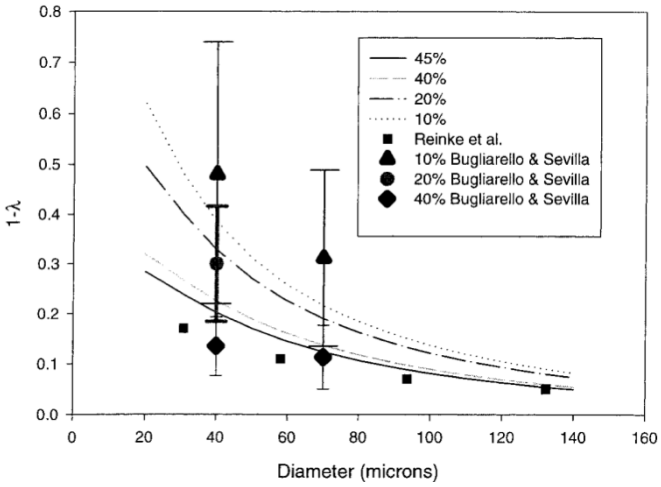

Figure 4: Peripheral plasma layer thickness vs. diameter, reproduced from Sharan and Popel (2001).

Bugliarello and Sevilla attribute the absence of any pulsatile effects to the nature of the flows being considered. As discussed, the characteristics of systems involving viscous fluids at low flow rates signify by definition low values of Reynolds numbers, and in light of their experiments, Bugliarello and Sevilla [11] conclude that the inertial effects of pulsatile flow are therefore "bound to be negligible".

2.4 Energy Minimisation Model

In attempting to explain the physical origins of the two-phase flow, Sharan and Popel theorize that the peripheral plasma layer provides a "lubricating region of lower viscosity" near the wall. They propose that, whilst the additional concentration of cells at the centre might dissipate additional energy, it is possible that this is counteracted by the reduced dissipation in the cell-free peripheral layer, and that the flow as a whole would dissipate less shear energy than if the erythrocytes were uniformly distributed. The observation is echoed by Reinke et al. [6], who propose that the viscosity reduction is due to an "alignment of deformed cells with the local flow profile".

This hypothesis of minimal shear energy dissipation has been suggested by various authors, however detailed quantitative studies are few, and concentrated almost exclusively on blood as a Newtonian fluid. The fundamental hypothesis is attractive, if only for its apparent simplicity and ready application to the problem at hand. Jeffery [19] applies the hypothesis when studying the viscosity of ellipsoid suspensions, but assumes a Newtonian fluid and does not consider the effect of shear-dependent viscosity. Deakin [20] considers the Casson fluid, but does not conduct a full quantitative investigation, stating inconclusively

that the hypothesis “may yet be involved in the pattern of particle distribution in blood flow”.

2.5 Force Balance Model

In 1961 Segré and Silberberg [3] observed that macroscopic spherical particles in laminar flow through straight tubes “collected in a thin, annular region” around the vessel centre. This phenomenon, termed the ’Segré-Silberberg’ or ’Tubular Pinch’ effect, has been documented as occurring predominantly at a radius of approximately $0.6R$ measured from the vessel centre. Also observed in the same publication are two other particle distributions, the first being the familiar cell-rich core described in section 2.3, and the second a more complex shape, as seen in Fig. 5.

Their experimental results have since been widely reproduced, first by Jeffrey et al. [21] and more recently by Matas et al. [22]. Moreover, the effect has been recognized as occurring over a wider range of conditions than in the original experiments, and has been associated with the aggregative behaviour observed in microvascular blood flow. Numerous theories have been suggested to explain the effect, including, amongst others, a mechanism of energy minimisation. However, the theory considered here is that originally suggested by Segré and Silberberg [3], concerning radial ’lift’ forces induced by the flow on individual particles. Shortly after the publication of Segré and Silberberg’s paper, Repetti and Leonard [23] provided a more rigorous analysis of the phenomenon. Through applying the Kutta-Joukowski theorem to the rotating erythrocytes in suspension, they concluded that the forces produced might be “of the correct order of magnitude to produce such a flow”, in reference to the observed annular formations. They propose that a particle-fluid velocity drag u_{diff} causes the velocity gradient to reverse in polarity at a point along the vessel radius, at which point the particles aggregate. However, the deduction is primarily qualitative, and no quantitative study has yet been undertaken. It is important to note that this hypothesis by itself does not provide a mechanism to establish the cell-rich core sought by this investigation, as without a dispersive force the particles will tend to a single position under the action of the lift force.

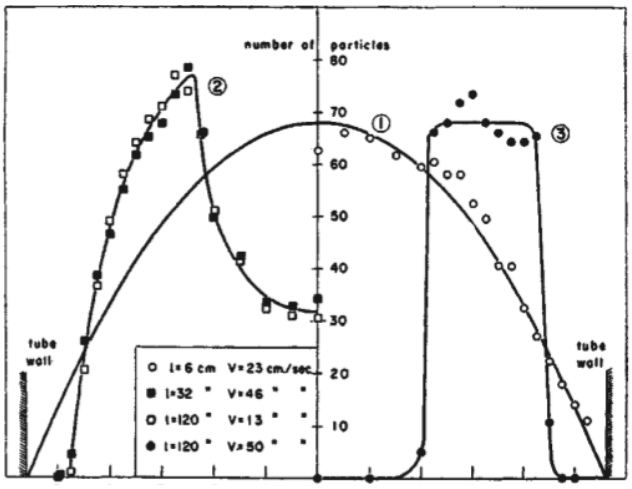

Figure 5: Local haematocrit distributions observed by Segré and Silberberg (1961).

A detailed analysis of the forces producing the observed distributions will be discussed in the following

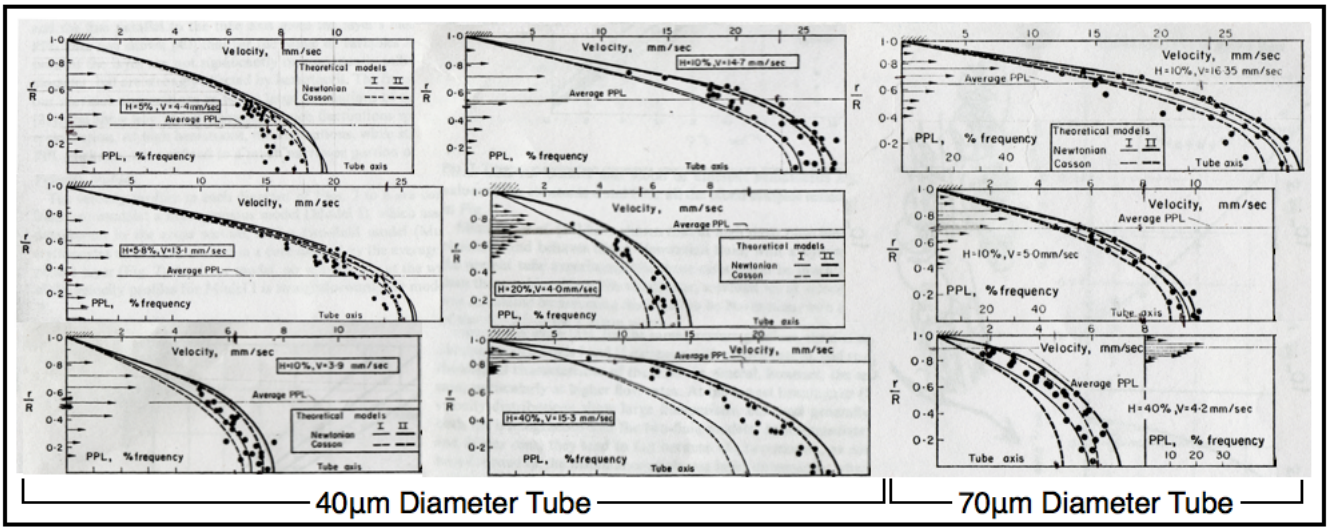

Figure 6: Velocity profiles reproduced from Bugliarello and Sevilla.

chapters. It is also useful to note that all previous work on the problem has concerned Pouiselle-type [24] flows of Newtonian fluids, and so the application of more complex fluids may provide an opportunity to yield more realistic results.

2.6 Experimental Data

In order to ascertain the validity and usefulness of the model, the predicted values of λ must be compared with *in vivo* data, of which the best is that obtained from Bugliarello and Sevilla [11]. In their paper, the authors published detailed results from their investigations, including velocity profiles and experimental conditions. From this data it is possible to match those experimental conditions to mathematical models, and therefore to directly compare the predicted against actual values of λ.

The parameters that are required as inputs to the models are Q, Q_c, the dimensionless total and core volumetric flow rates and α, the core to plasma viscosity ratio. Bugliarello and Sevilla published the nine velocity profiles shown in Fig. 6, to which Simpson's Rule can be applied to estimate the values of q and q_c. In order to deduce the dimensionless flow rates however, values for η and τ_y are required.

In the Casson model, the parameters η and τ_y are functions of haematocrit, for which Bugliarello and Sevilla [11] publised two plots. The parameters can be approximated by two linear interpolations, where the agreement between the interpolated functions and original data is shown in Fig 7. The parameters can thus be implemented in the model as functions of haematocrit H, as from the linear fits:

$$\tau_y(H) = \frac{1}{10}(0.025 + 0.4375H)^2 \qquad and \qquad \eta(H) = \frac{1}{10}(0.12 + 0.2H)^2 \tag{6}$$

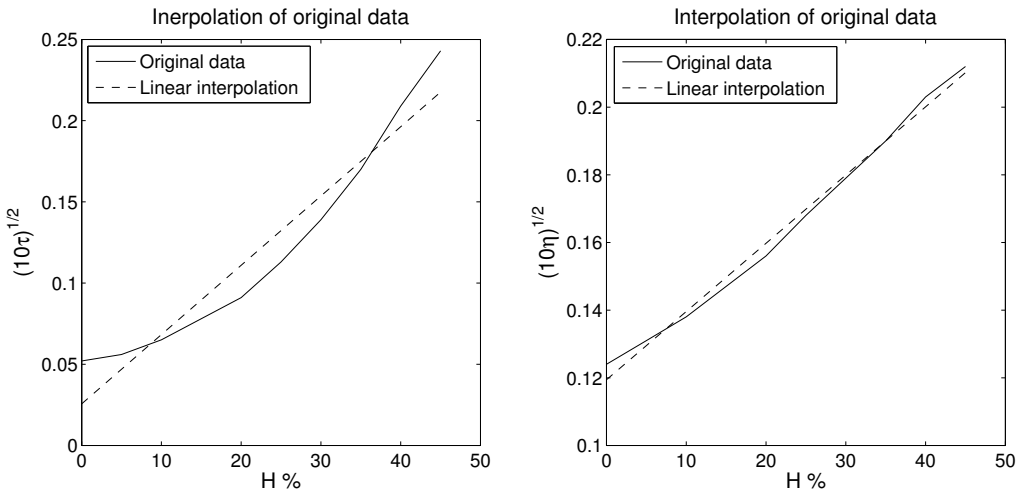

Figure 7: Interpolation of Casson parameters against original data

H(%)	R(μm)	V(mm/s)	Q	λ
5	20	4.41	185.34	0.34
5.8	20	13.11	374.16	0.34
10	20	3.91	168.52	0.52
10	20	14.71	681.02	0.54
20	20	4.03	130.33	0.69
40	20	15.38	313.71	0.81
10	35	16.35	578.85	0.65
10	35	5.04	231.89	0.70
40	35	4.25	52.56	0.90

(a) Experimental data from Bugliarello and Sevilla.

Hc(%)	τ(N/m^2)	η(Ns/m^2)	α	Qc
23.80	0.0017	0.0028	1.95	38.87
27.60	0.0021	0.0031	2.13	99.46
23.22	0.0016	0.0028	1.92	72.57
21.73	0.0014	0.0027	1.86	313.41
30.50	0.0025	0.0033	2.28	85.42
49.60	0.0059	0.0048	3.34	253.00
16.50	0.00094	0.0023	1.63	351.43
12.74	0.00065	0.0021	1.47	1821.99
46.10	0.0051	0.0045	3.13	45.64

(b) Data deduced from experimental data.

Table 1: Table showing data obtained from Bugliarello and Sevilla.

where H is the local haematocrit. The haematocrit values quoted in Fig. 6 are the tube haematocrit values, which represent the time independent averages taken over the vessel. In order to obtain the core haematocrit H_c, a mass balance is imposed on the flow:

$$H_c = H_T \frac{Q}{Q_c} \tag{7}$$

Since the total and core volumetric flow rates can be extracted as described earlier, the core haematocrit can therefore be deduced allowing the Casson parameters to be calculated. Table 1 shows the data calculated from Bugliarello and Sevilla [11]. Note that the typical Reynolds numbers $Re = \frac{\rho U D}{\eta}$ are on the order of $\approx 1 \times 10^{-2}$, confirming that the flows are comfortably within the laminar region as assumed.

2.7 Overview

Sections 2.4 and 2.5 introduced two mechanisms whereby a phase-separation may be be achieved, and Section 2.2 described the fluid models most relevant to the modelling of blood. Section 2.6 provides a detailed source of experimental data by which to compare the predictions of the models.

Chapter 3 will therefore proceed to apply firstly a minimisation of shear energy to the fluid models discussed, beginning with the elementary case of a Newtonian fluid. This analysis will consider the fluid to exist in two phases as previously discussed, with a cell-rich core layer separated from a peripheral cell-free layer at a radial position λ.

Chapter 4 will consider the forces affecting individual particles, and their effects on the same models of fluid analyzed. In this case, the fluid will be considered as a uniform model with the distribution of local haematocrit H as continuous. The two-phase behaviour will then be deduced from the resulting distributions.

Before developing any mathematical model, it is important to establish explicitly the physical assumptions on which it will be based. The following investigation makes the following three for the purpose of simplicity:

1. *Rigid, neutrally buoyant particles* - Gravity, and therefore the orientation of the vessel has no effect on the distribution of erythrocytes. Shear dissipation related to cell deformation is not considered.

2. *Fully developed, steady state flow* - Inertial and pulsatile effects will be ignored, and it will be assumed that the vessel is sufficiently long to allow the particles to achieve an equilibrium migration.

3. *Small diameter vessels of 50-300μm* - Any expressions adapted from literature will be used only within their established limits of operation.

The ultimate purpose of this investigation is to better understand the mechanisms governing the two-phase separation in the microvasculature. Predictions made by the models are compared with existing in vitro data, and their validity assessed.

3 Energy Minimisation Model

The first part of this investigation is an attempt to develop a model that will predict the radial position of the phase boundary, based on the principle of minimal shear energy dissipation. In any fluid there is an

associated fluid viscosity, which in a moving fluid induces shear forces proportional to:

$$\tau = \eta \frac{\partial u}{\partial r} \tag{8}$$

where η is the dynamic viscosity, u the axial fluid velocity and r the radial co-ordinate. These shear forces dissipate energy at a rate per unit axial length, given by the following expression taken from Lubansky [25]:

$$\dot{E}_s = \int_0^R 2\eta\pi\dot{\gamma}^2 r dr \tag{9}$$

in a cylindrical vessel where $\dot{\gamma} = \frac{\partial u}{\partial r}$ is the radial velocity gradient. A two-phase model of flow will be considered, separated at a phase boundary at $\xi = \lambda$, where $\xi = \frac{r}{R}$ denotes the dimensionless radial co-ordinate. These two phases will have differing physical properties, and it is possible that there exists a radial distance λ for which the rate of energy dissipation is minimised. This chapter will investigate the validity of this hypothesis through the application of the above expression to both the power-law fluid family and the Casson fluid.

3.1 Newtonian Fluid

In a Newtonian fluid, the viscosity η in Eq. 8 is taken as a constant, and the dimensionless flow behaviour index $n = 1$. Beginning with the Navier-Stokes equations, the velocity profiles describing the flow can be derived, ignoring inertial forces due to the fully developed and steady state nature of the flow. Applying the no-slip condition to the wall of the vessel $u_p|_{r=R} = 0$, yields:

$$u_p = \frac{P}{4\mu_p}\left(R^2 - r^2\right) \tag{10}$$

Where $P = -\frac{\partial p}{\partial z}$ is a positive quantity representing the pressure gradient driving the flow and u_p is the velocity in the plasma layer. Secondly, the velocity profile must be continuous over the boundary, and so $u_c|_{r=r_p} = u_p|_{r=r_p}$, where u_c is the core velocity, yields:

$$u_c = \frac{P}{4\eta_p}\left(\left(R^2 - r_p^2\right) + \frac{\eta_p}{\eta_c}\left(r_p^2 - r^2\right)\right) \tag{11}$$

Substituting in the non-dimensional radial co-ordinate $\xi = \frac{r}{R}$ and $\lambda = \frac{r_p}{R}$, the complete velocity profile is:

$$u(\xi) = \begin{cases} \frac{PR^2}{4\eta_p}\left(1-\xi^2\right), & \lambda < \xi < 1 \\ \frac{PR^2}{4\eta_p}(\left(1-\lambda^2\right) + \frac{\eta_p}{\eta_c}\left(\lambda^2-\xi^2\right)), & 0 < \xi < \lambda \end{cases} \tag{12}$$

These expressions can be substituted into Eq. 9. Introducing the core to plasma viscosity ratio $\alpha = \frac{\eta_c}{\eta_p}$, and the constant $C = \frac{PR^4}{\eta_p}$ gives:

$$\dot{E}_s = 2\pi(\frac{PR^2}{4\eta_p})^2\eta_p\left[\lambda^4\left(\frac{\eta_p}{\eta_c}-1\right)+1\right] = 2\pi C^2\eta_p\left[\lambda^4\left(\frac{1}{\alpha}-1\right)+1\right] \tag{13}$$

Finally, differentiating with respect to λ yields:

$$\frac{\partial\dot{E}}{\partial\lambda} = 8\pi C^2\eta_p\lambda^3(\frac{1}{\alpha}-1) = 0 \tag{14}$$

This gives the trivial result that $\lambda = 0$ for a minimum, or that $\alpha = 1$, suggesting therefore that for a Newtonian fluid the rate of shear energy dissipation will be minimised when the fluid is of a uniform viscosity. In physical terms, this signifies that the erythrocytes should adopt a uniform distribution throughout the vessel, which contrasts with observations. Before however abandoning the Newtonian model, the more fundamental circumstance of the physiology should be considered. The analysis attempted to optimize the shear energy for a constant pressure gradient, and whilst this condition might be important, it is perhaps not the most valuable attribute physiologically.

From the perspective of nutrient supply and waste removal, it might be that the circulatory system would seek to maximise the blood flow rate. The next section therefore attempts to minimize the shear energy of the flow when subject to a constant total flow rate q.

3.1.1 Constant Total Volumetric Flow Rate

In order to optimize the flow for a constant volume flow rate, an expression for q is needed in terms of P. Integrating across the cross section of the vessel gives:

$$q = 2\pi R^2\int_0^\lambda u_c(\xi)\xi d\xi + 2\pi R^2\int_\lambda^1 u_p(\xi)\xi d\xi = \frac{\pi R^2 C}{2}(\lambda^4(\frac{1}{\alpha}-1)+1) \tag{15}$$

Substituting Eq. 15 into Eq. 13 to obtain the expression for energy in terms of a constant flow rate, and again differentiating with respect to λ and equating to zero gives:

$$\dot{E}_s = \frac{8q^2\eta_p}{\pi R^4}\frac{1}{\lambda^4(\frac{1}{\alpha}-1)+1} \tag{16}$$

$$\frac{d\dot{E}_s}{d\lambda} = \frac{-8q^2\eta_p}{\pi R^4}\frac{4\lambda^3(\frac{1}{\alpha}-1)}{(\lambda^4(\frac{1}{\alpha}-1)+1)^2} = 0 \tag{17}$$

As before, $\lambda^3(\frac{1}{\alpha}-1) = 0$, which is a trivial result. However, considering that the erythrocytes are only carried in the core of the flow, it may be more relevant to optimize the flow with regards to the constant core flow rate q_c.

3.1.2 Constant Core Volumetric Flow Rate

Similar to the previous analysis, the core volumetric flow rate q_c can be expressed in terms of the pressure gradient, by integrating the velocity profile over the core region:

$$q_c = 2\pi R^2 \int_0^\lambda u_c(\xi)\xi d\xi = \pi R^2 C\left(\lambda^4(\frac{1}{2\alpha}-1)+\lambda^2\right) \tag{18}$$

Again, substituting into the shear energy dissipation equation:

$$\dot{E}_s = \frac{2\eta_p q_c^2}{\pi R^4}\frac{\left(\lambda^4(\frac{1}{\alpha}-1)+1\right)}{\left(\lambda^4(\frac{1}{2\alpha}-1)+\lambda^2\right)^2} \tag{19}$$

And differentiating with respect to λ gives:

$$\frac{d\dot{E}_s}{d\lambda} = \frac{4\lambda^3\left(\frac{1}{\alpha}-1\right)}{\left(\lambda^2+\lambda^4\left(\frac{1}{2\alpha}-1\right)\right)^2} - \frac{2\left(2\lambda+4\lambda^3\left(\frac{1}{2\alpha}-1\right)\right)\left(1+\lambda^4\left(\frac{1}{\alpha}-1\right)\right)}{\left(\lambda^2+\lambda^4\left(\frac{1}{2\alpha}-1\right)\right)^3} = 0 \tag{20}$$

Substituting $a = \frac{1}{\alpha}-1$ and $b = \frac{1}{2\alpha}-1$ and re-arranging, this can be expressed as a depressed cubic, where $t = \lambda^2$:

$$t^3 + \frac{2}{a}t + \frac{1}{ab} = 0 \tag{21}$$

This form can be solved analytically using Cardano's method [26], producing two non-trivial positive real results, as shown in Fig. 8.

As can be seen, the first root is positive and real, but is outside the vessel radius and so can be discarded as being physically invalid. The second however shows that there does indeed exist a value of λ for which

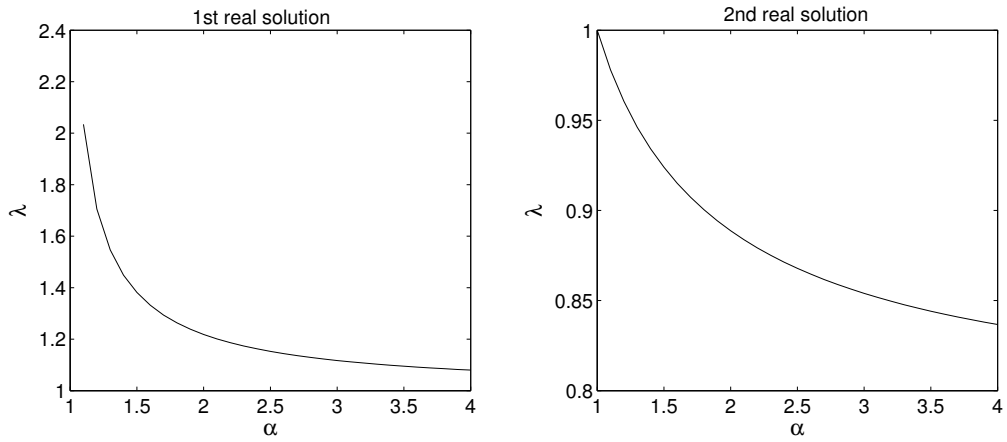

Figure 8: α vs. λ for a Newtonian fluid, shear energy minimisation at constant q_c.

the shear energy dissipation is either maximized or minimised for any given value of core flow rate q_c. By observing the plot of energy distribution across the vessel, it is confirmed that this point corresponds to a minimum, affirming the validity of the solution.

The results suggest that for an increasing core viscosity (increasing α), the thickness of this layer will decrease in order to provide the most energy efficient erythrocyte supply. Having now established that the minimum energy hypothesis does indeed provide physically realistic results, the next step in the analysis is to consider more realistic fluid models, and to compare the results with *in vivo* data.

3.2 General Power-Law Fluids

To investigate the applicability of this model, the analysis will proceed in a similar manner to the previous. Firstly, the velocity profiles describing the generalized fluid must be derived. The driving pressure acting on a circular element of fluid can be equated to the shear stress acting at its perimeter, and so substituting the power law expression for τ from Eq. 1 and rearranging gives:

$$\frac{\partial u}{\partial r} = -r^{\frac{1}{n}} \left(\frac{P}{2K} \right)^{\frac{1}{n}} \tag{22}$$

The boundary conditions imposed upon the flow will be identical to the Newtonian case. The no-slip and continuity conditions, once again expressed as $u_p|_{r=R} = 0$ and $u_c|_{r=r_p} = u_p|_{r=r_p}$ yield:

$$u(\xi) = \begin{cases} \left(\frac{PR}{2K_p}\right)^{\frac{1}{n_p}} \left(R\frac{n_p}{n_p+1}\right) \left(1^{\frac{n_p+1}{n_p}} - \xi^{\frac{n_p+1}{n_p}}\right), & \lambda < \xi < 1 \\ \left(\frac{PR}{2K_c}\right)^{\frac{1}{n_c}} \left(R\frac{n_c}{n_c+1}\right) \left(\lambda^{\frac{n_c+1}{n_c}} - \xi^{\frac{n_c+1}{n_c}}\right) + \left(\frac{PR}{2K_p}\right)^{\frac{1}{n_p}} \left(R\frac{n_p}{n_p+1}\right) \left(1^{\frac{n_p+1}{n_p}} - \lambda^{\frac{n_p+1}{n_p}}\right), & 0 < \xi < \lambda \end{cases} \tag{23}$$

where the subscripts c and n refer to the core and plasma layers respectively. Substituting into the shear energy equation:

$$\dot{E}_s = 2\pi R^2 \left(\frac{\lambda^{3+\frac{1}{n_c}}}{3+\frac{1}{n_c}} \right) K_c \left(\frac{PR}{2K_c} \right)^{\frac{n_c+1}{n_c}} + 2\pi R^2 \left(\frac{1-\lambda^{3+\frac{1}{n_p}}}{3+\frac{1}{n_p}} \right) K_p \left(\frac{PR}{2K_p} \right)^{\frac{n_p+1}{n_p}} \tag{24}$$

Note that at this point, the pressure terms have different exponents and so cannot be factored out. However, differentiating with respect to λ and equating to zero results in:

$$\lambda = \frac{2}{RP} \left(\frac{K_c^{n_p}}{K_p^{n_c}} \right)^{\frac{1}{n_p - n_c}} \tag{25}$$

It is not clear however whether this result represents a maximum or minimum rate of energy dissipation, and this must be determined to ascertain the validity of the solution. Eq. 25 can be differentiated twice with respect to λ to obtain:

$$\frac{d^2\dot{E}_s}{d\lambda^2} = L\pi PR^3\lambda \left\{ \left(\frac{2n_c+1}{n_c} \right) \left(\frac{PR\lambda}{2} \right)^{\frac{1}{n_c}} \left(\frac{1}{K_c} \right)^{1+\frac{1}{n_c}} - \left(\frac{2n_p+1}{n_p} \right) \left(\frac{PR\lambda}{2} \right)^{\frac{1}{n_p}} \left(\frac{1}{K_p} \right)^{1+\frac{1}{n_p}} \right\} \tag{26}$$

The second differential must equal a positive value to produce a minimum energy rate of energy dissipation. Substituting Eq. 25 into the above expression, it is possible to obtain:

$$\frac{K_p}{K_c} > \frac{2n_c+\beta}{2n_c+1} \tag{27}$$

where $\beta = \frac{n_c}{n_p}$ is the ratio of the core to plasma dimensionless flow behaviour indices. It is assumed as previously that the core viscosity is greater than the plasma, and so the ratio $\frac{K_c}{K_p} > 1$. Clearly, it is possible that when $\beta > 1$, the solution is capable of producing a physically valid solution.

3.2.1 Constant Total Volumetric Flow Rate

Next, the optimisation is investigated for a constant volumetric flow rate. Making the substitutions $A = \left(\frac{2K}{PR}\right)^{\frac{1}{n}}$ and $B = \left(\frac{n+1}{n}\right)$, the flow rate q is obtained as:

$$q = 2\pi R^3 \left\{ \frac{\lambda^2}{2} \left(\frac{B_c^2 \lambda^{B_c}}{A_c\left(2+B_c\right)} + \frac{B_p\left(1-\lambda^{B_p}\right)}{A_p} \right) - \frac{B_p\left(B_p\left(\lambda^2-1\right) - 2\lambda^2\left(\lambda^{B_p}-1\right)\right)}{2A_p\left(2+B_p\right)} \right\} \tag{28}$$

It is clear from this expression that it is not possible to isolate the pressure gradient P in terms of a flow

rate whilst the two phases are allowed different values for their flow behaviour indices n. In order to proceed with the investigation, the simplifying assumption that $n_p = n_c$ is made, noting that the case where $n_c \neq n_p$ warrants further investigation that was not possible due to time constraints.

Eq. 29 is therefore obtained for q. Note that in the case where $n = 1$, Eq. 15 is recovered as derived in the previous Newtonian case. The ratio of the flow consistency indices $\varepsilon = \left(\frac{K_c}{K_p}\right)^{\frac{1}{n}}$ is introduced to obtain:

$$q = \pi R^3 \left(\frac{PR}{2K_p}\right)^{\frac{1}{n}} \lambda^2 \left\{\frac{B^2\lambda^2}{\varepsilon\left(B+2\right)} + B\left(1-\lambda^B\right)\right\} \tag{29}$$

Setting $n_p = n_c$ in Eq. 24 yields:

$$\dot{E}_s = \left(2\pi R^2\right)\left(\frac{K_p}{3+\frac{1}{n}}\right)\left(\frac{PR}{2K_p}\right)^{\frac{n+1}{n}}\left[\frac{\lambda^{3+\frac{1}{n}}}{\varepsilon} + \left(1-\lambda^{3+\frac{1}{n}}\right)\right] \tag{30}$$

Finally, substituting in Eq. 29 and eliminating $\frac{PR}{K_p}$ gives:

$$\frac{\dot{E}_s}{\gamma_1\gamma_2\gamma_3} = \frac{1}{\left(\lambda^{B+2}\left(\varepsilon-1\right)+1\right)^n} \tag{31}$$

Where the constants $\gamma_1 = 2\pi\left(\frac{R^{3+\frac{1}{n}}}{3+\frac{1}{n}}\right)$, $\gamma_2 = K_p\left(\frac{q}{\pi R^{B+2}}\right)^{n+1}$ and $\gamma_3 = \left(\frac{(B+2)}{B^2}\right)^{n+1}$. This again reduces to the equivalent Newtonian expression when $n = 1$. Finally, this expression can be differentiated with respect to λ and equated to zero to obtain the shear energy minimisation:

$$\frac{1}{\gamma_1\gamma_2\gamma_3}\frac{d\dot{E}_s}{d\lambda} = -\left(3+\frac{1}{n}\right)n\left(\varepsilon-1\right)\lambda^{2+\frac{1}{n}}\left(1+\left(\varepsilon-1\right)\lambda^{3+\frac{1}{n}}\right)^{-1(1+n)} = 0 \tag{32}$$

And therefore $\lambda^{2+\frac{1}{n}} = 0$. This is consistent with the result for the Newtonian case, and it is clear therefore that for any member of the power-law fluid family, there exists no value of λ for which shear energy dissipation is minimised for a constant volume flow rate. The minimisation will thus next be analyzed for a constant core flow rate, as a similar approach yielded promising results in the case where $n = 1$.

3.2.2 Constant Core Volumetric Flow Rate

Similarly to the previous Newtonian analysis, an expression is required to eliminate the pressure gradient P in favour of the constant core flow rate q_c. Integrating the velocity profile over the core region yields:

$$q_c = \pi R^3\left(\frac{PR}{2K_p}\right)\lambda^2 B\left\{\frac{\lambda^2}{\varepsilon\left(B+2\right)} + \left(1-\lambda^B\right)\right\} \tag{33}$$

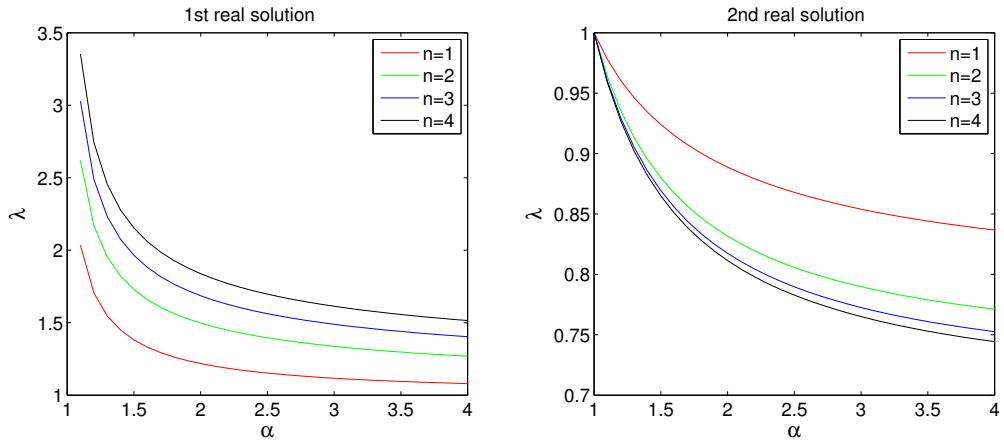

Figure 9: α vs. λ for a power law fluids of varying flow consistency index n, shear energy minimisation at constant q_c.

Substituting into Eq. 30 and again eliminating $\frac{PR}{2K_p}$:

$$\frac{1}{\gamma_1\gamma_2\gamma_3}\dot{E}_s = \left\{\frac{\lambda^{3+\frac{1}{n}}}{\varepsilon} + \left(1-\lambda^{3+\frac{1}{n}}\right)\right\}\left\{\frac{1}{\frac{\lambda^{B+2}}{\varepsilon} + \frac{\lambda^2}{B}(B+2)(1-\lambda^B)}\right\}^{n+1} \tag{34}$$

Finally, differentiating and equating to zero gives:

$$\begin{aligned}&\left(3+\tfrac{1}{n}\right)\lambda^B\left(\tfrac{1}{\varepsilon}-1\right)\left(\lambda^{B+2}\left(\tfrac{B}{\varepsilon}-(B+2)\right)+\lambda^2(B+2)\right)\\ &-\left(\lambda^B(B+2)\left(\tfrac{B}{\varepsilon}-(B+2)\right)+2(B+2)\right)\left(\lambda^{B+2}\left(\tfrac{1}{\varepsilon}-1\right)+1\right)=0\end{aligned} \tag{35}$$

This expression is now solved numerically using MatLab, over a range of $n = 1, 2, 3, 4$ and $\alpha = 1 : 4$, noting that $\varepsilon = \alpha^{\frac{1}{n}}$. The results are shown in Fig. 9.

Again, there are two real solutions for λ, although the first solution can be discarded as being unphysical. The second real solution however suggests that the thickness of the core layer decreases with increasing flow consistency index. This agrees with the velocity profiles of the flows, which show that as n decreases, the core velocity increases, shown in Fig. 10, serving to preserve a constant mass flow rate. Note that the Newtonian case observed previously is recovered when $n = 1$.

3.2.3 Results and Discussion

The analysis so far has established that the hypothesis of minimum shear energy dissipation shows promise as a possibly valid approach to determining the location of the phase boundary layer. The method predicts values for λ that are physically realistic, and thus the behaviour of λ with varying α predicted by the power-law fluid model can now be compared with that of existing data.

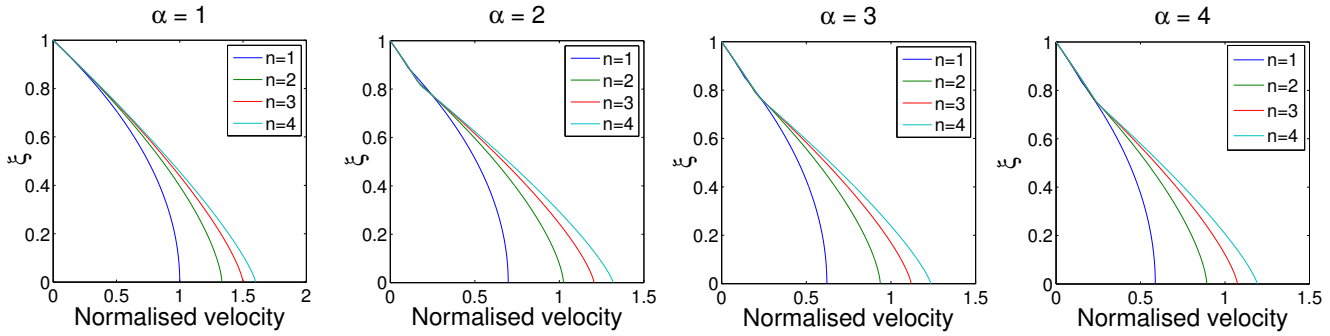

Figure 10: Velocity profiles for power law fluids of varying flow consistency index n.

When comparing their data with that of Bugliarello and Sevilla and Reinke et al., Sharan and Popel state that "as expected, (the) thickness of the cell-free layer decreases as haematocrit increases", shown ealier in Fig. 4. This is an interesting result, as a superficial comparison of the model with the experimental data shown would suggest that an increase in tube haematocrit leads to a decrease in core viscosity, whilst intuitively it might be expected that the viscosity would increase with haematocrit, as a higher haematocrit would signify a higher erythrocyte density. This reduction in viscosity at small vessel diameters shown by the model is consistent with the Fåhreaus-Lindqvist Effect.

However, the results of the analysis show that the power-law fluid model developed does not have the capacity to model the Fåhreaus-Lindqvist effect comprehensively, as the values of λ predicted by the model have no dependence on vessel radius R. The results obtained cannot therefore be directly compared to that presented by Sharan and Popel. This can be attributed to a limitation of the fluid model, as the Newtonian model has no inherent shear dependent behaviour. Any dependence on the vessel radius in the general power-law model, whilst originally present, is factored out when equating $n_c = n_p$. The next chapter will therefore proceed with the application of the energy minimisation to a more complex fluid model.

3.3 Casson Fluid

The yield-stress introduced by the Casson equation creates a problem when attempting to derive the relevant velocity profiles, and so a linear piece-wise approximation is made for the discontinuous shear profile τ, comprised of two sections as shown in Fig. 11. Firstly, a steep linear region is introduced to replace the step in the original shear stress function. The gradient of the line is taken to be $\frac{1}{\epsilon}$, where ϵ is small. As $\epsilon \to 0$, the approximation approaches the axis and therefore the original function. The second region behaves like the original Casson equation where $K = \sqrt{\eta}$, an effective viscosity term is

susbtituted. Eq. 3 is modified to account for the fact that in this case both the radial velocity gradient $\frac{\partial u}{\partial r}$ and shear stress τ are negative with respect to positive axial flow u. The intersection between the two segments therefore occurs at $\tau = \tau_c$, which is determined as:

$$\therefore \sqrt{-\tau_c} = \frac{\sqrt{\tau_y}}{1 - \sqrt{\epsilon\eta}} \tag{36}$$

The shear stress profiles can therefore be expressed as:

$$\sqrt{-\tau} = \begin{cases} \sqrt{\tau_y} + \sqrt{-\eta\dot{\gamma}} & \infty < \dot{\gamma} < -\tau_c\epsilon \\ \sqrt{\frac{-\dot{\gamma}}{\epsilon}} & -\tau_c\epsilon < \dot{\gamma} < 0 \end{cases} \tag{37}$$

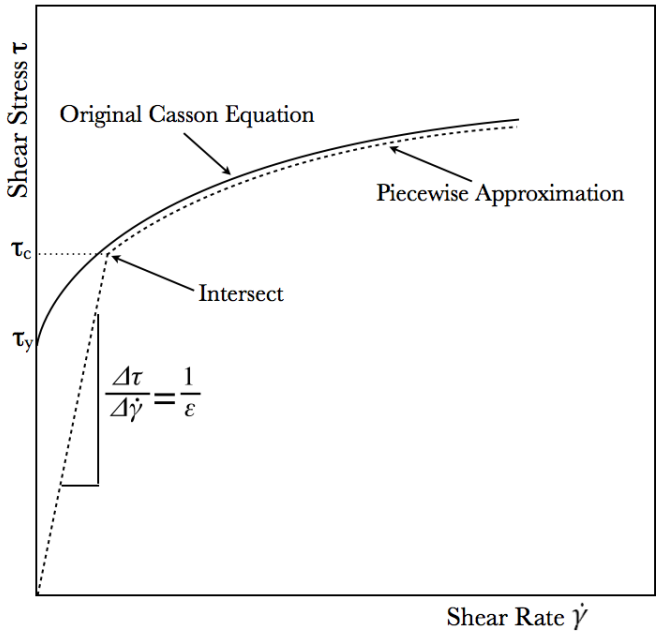

Figure 11: τ vs. $\dot{\gamma}$ for a Casson fluid.

Balancing forces on the fluid, $\tau = \frac{-Pr}{2}$ is obtained yielding an expression for the plug flow boundary:

$$\tau_s = \frac{\dot{\gamma}_s}{\epsilon} = \frac{-Pr}{2} \tag{38}$$

$$\dot{\gamma}_s = \frac{\partial u_s}{\partial r} = \frac{\partial u_s}{\partial \xi}\frac{1}{R} \tag{39}$$

$$u_s = -\frac{\epsilon P R^2}{4}\xi^2 + A_s \tag{40}$$

where the subscript s to denotes plug flow properties. Continuing for the Casson flow region and substituting into Eq. 3:

$$\dot{\gamma}_c = \frac{\partial u_c}{\partial \xi}\frac{1}{R} = -\frac{\left(\sqrt{-\tau_c} - \sqrt{\tau_y}\right)^2}{\eta} = \frac{1}{\eta}\left(\frac{-PR}{2}\xi + 2\sqrt{\frac{PR}{2}}\sqrt{\tau_y}\sqrt{\xi} - \tau_y\right) \tag{41}$$

$$u_c = \frac{-PR^2}{2\eta}\frac{\xi^2}{2} + \frac{4}{3}\sqrt{\frac{PR^3\tau_y}{2\eta^2}}\xi^{\frac{3}{2}} - \frac{\tau_y R}{\eta}\xi + A_c \tag{42}$$

Finally, in the peripheral plasma region, where Newtonian flow is assumed:

$$u_p = -\frac{PR^2}{4\eta_p}\xi^2 + A_p \tag{43}$$

Applying the no-slip condition to the peripheral region yields:

$$\therefore u_p = \frac{PR^2}{4\eta_p}\left(1-\xi^2\right) \tag{44}$$

Applying continuity of velocity at the core-plasma phase boundary yields:

$$u_c = \frac{PR^2}{4\eta}\left(\lambda^2\left(1-\alpha\right)-\left(\xi^2-\alpha\right)\right) - \frac{4}{3}\sqrt{\frac{PR^3\tau_y}{2\eta^2}}\left(\lambda^{\frac{3}{2}}-\xi^{\frac{3}{2}}\right)+\frac{\tau_y R}{\eta}\left(\lambda-\xi\right) \tag{45}$$

Where the ratio $\alpha = \frac{\eta}{\eta_p}$ is introduced to denote the effective core-plasma viscosity ratio. Finally, continuity can be applied at the plug-core boundary, which is denoted λ_p:

$$\therefore u_s = \frac{\epsilon PR^2}{4}\left(\lambda_p^2-\xi^2\right)+\frac{PR^2}{4\eta}\left(\lambda^2\left(1-\alpha\right)-\left(\lambda_p^2-\alpha\right)\right) - \frac{4}{3}\sqrt{\frac{PR^3\tau_y}{2\eta^2}}\left(\lambda^{\frac{3}{2}}-\lambda_p^{\frac{3}{2}}\right)+\frac{\tau_y R}{\eta}\left(\lambda-\lambda_p\right) \tag{46}$$

Before proceeding with the analysis, it is useful to non-dimensionalize these quantities. The dimensionless pressure gradient $\theta = \sqrt{\frac{\tau_y}{2PR}}$ is introduced, and the profiles can therefore be expressed:

$$U\left(\xi\right) = \begin{cases} \frac{\alpha}{4}\left(1-\xi^2\right) & 1<\xi<\lambda \\ \frac{1}{4}\left(\lambda^2\left(1-\alpha\right)-\left(\xi^2-\alpha\right)\right)-\frac{4}{3}\theta\left(\lambda^{\frac{3}{2}}-\xi^{\frac{3}{2}}\right)+2\theta^2\left(\lambda-\xi\right) & \lambda<\xi<\lambda_p \\ \frac{\epsilon}{4}\left(\lambda_p^2-\xi^2\right)+U_c\left(\lambda_p\right) & \lambda_p<\xi<0 \end{cases} \tag{47}$$

where the dimensionless velocity is denoted by $U = u\left(\frac{\eta}{PR^2}\right)$. The viscosity of the plug layer has been taken as equivalent to that of the core layer, when in reality, it's viscosity will be infinite as it flows as a solid. This behaviour is incorporated into the small value assigned to ϵ.

The plug flow boundary occurs at the point where the applied shear stress equals the yield limit. In this approximation however, the boundary will occur where $\tau = \tau_c$, the intersection of the two segments. Using the expression in Eq. 36 derived previously, the value of ξ this point is found to be:

$$\tau = \tau_c = \frac{-PR}{2}\lambda_p = \frac{-\tau_y}{\left(1-\sqrt{\eta\epsilon}\right)^2} \tag{48}$$

$$\lambda_p = \frac{2\tau_y}{PR}\left(\frac{1}{1-\sqrt{\eta\epsilon}}\right)^2 = \frac{4\theta^2}{\left(1-\sqrt{\eta\epsilon}\right)^2} \tag{49}$$

In order to substitute into the shear energy equation, the effective viscosity of the Casson region must be

defined. Comparing it to the Newtonian form:

$$\eta_c = \frac{\tau_c}{\dot{\gamma}_c} = -\frac{\left(\tau_y + 2\sqrt{\tau_y}\sqrt{-\eta\dot{\gamma}_c} - \eta\dot{\gamma}_c\right)}{\dot{\gamma}_c} = \eta - 2\sqrt{\frac{\eta\tau_y}{-\dot{\gamma}_c}} - \frac{\tau_y}{\dot{\gamma}_c} \tag{50}$$

or, in non-dimensional form where the non-dimensional velocity gradient $\dot{\Gamma} = \dot{\gamma}\left(\frac{\eta}{PR}\right)$ and non-dimensional viscosity $\Pi_c = \frac{\eta_c}{\eta}$ are introduced:

$$\Pi_c = \frac{\eta_c}{\eta} = 1 - \frac{2\theta}{\left(-\frac{\Gamma_c}{2}\right)^{\frac{1}{2}}} + \frac{\theta}{\left(-\frac{\Gamma_c}{2}\right)} \tag{51}$$

The shear energy equation can be similarly non-dimensionalized to give:

$$\dot{\Sigma}_s = \dot{E}_s\left(\frac{\eta}{2\pi P^2 R^4}\right) = \int_0^1 \Pi\dot{\Gamma}^2\xi d\xi \tag{52}$$

The velocity profiles can be substituted into Eq. 52 to give:

$$\dot{\Sigma}_s = \frac{1}{16}\epsilon\eta\lambda_p + \frac{1}{16}\left(\lambda^4 - \lambda_p^4\right) - \frac{2\theta}{7}\left(\lambda^{\frac{7}{2}} - \lambda_p^{\frac{7}{2}}\right) + \frac{\theta}{3}^2\left(\lambda^3 - \lambda_p^3\right) + \frac{\alpha}{16}\left(1 - \lambda^4\right) \tag{53}$$

Lastly, differentiating and equating to zero yields:

$$\frac{d\dot{\Sigma}_s}{d\lambda} = \frac{1}{4}\left(1-\alpha\right)\lambda^3 - \theta\lambda^{\frac{5}{2}} + \theta^2\lambda^2 = 0 \tag{54}$$

$$\lambda = \left(\frac{2\theta}{1-\alpha}\right)^2\left(1 \pm \sqrt{\alpha}\right)^2 \tag{55}$$

So the minimisation in the case of a Casson fluid does produce a non-trivial solution for λ. Again, in order to be a physically valid solution, it must be both within the vessel boundary and a local minimum of shear dissipation, rather than a maximum. For the solution to be a minimum, the second differential of the shear energy equation must be greater than zero:

$$\frac{d^2\dot{\Sigma}_s}{d\lambda^2} = \frac{3}{4}\left(1-\alpha\right)\lambda^2 - \frac{5}{2}\theta\lambda^{\frac{3}{2}} + 2\theta^2\lambda > 0 \tag{56}$$

Figure 12a shows a plot of both solutions obtained from Eq. 55 fo a value of $\theta = 0.1$. It can be seen that the $\left(1 - \sqrt{\alpha}\right)^2$ solution produces values of λ exclusively within the plug-flow region, so this solution can

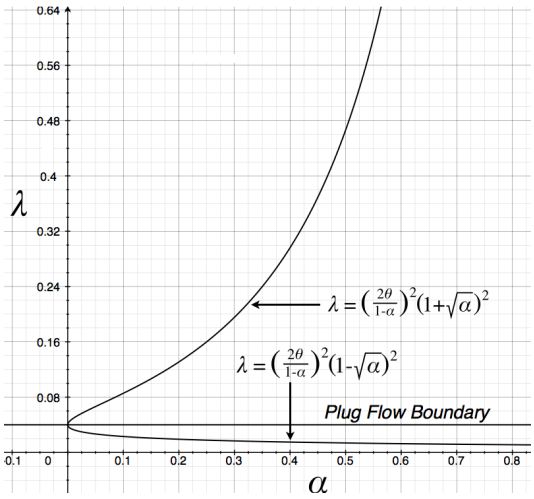

(a) Both solutions for λ, $\theta = 0.1$.

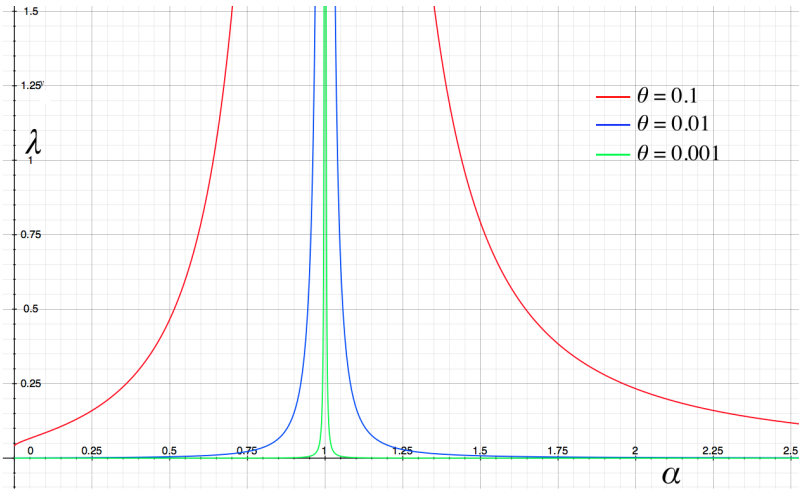

(b) Plot showing the effect of θ on λ.

Figure 12

therefore be discarded. The only physically possible solution is therefore:

$$\lambda = \left(\frac{2\theta}{1-\alpha}\right)^2 \left(1+\sqrt{\alpha}\right)^2 \tag{57}$$

Figure 12b shows the effect of varying θ. The largest theoretical value of $\theta = 0.5$, as this would cause the λ_p to lie at the vessel wall. The solution for λ tends to zero as the non-dimensional pressure gradient θ decreases, which makes intuitive sense in the absence of flow induced shear stress.

The investigation only considers values of $\alpha > 1$ as the erythrocyte core is assumed to be more viscous than the peripheral layer. It can be seen that all three values of θ produce λ values that lie within the vessel boundary.

Substituting Eq. 57 into Eq. 56 however reveals that for $\alpha > 1$, the solutions are maxima and are therefore not valid. This signifies that for a Casson fluid flowing under a constant pressure gradient, neither of the solutions above produce solutions for λ that satisfy both conditions and are therefore not physically valid, agreeing with previous analysis of this form. The next section will thus proceed to investigate the case of a constant volumetric flow rate.

3.3.1 Constant Total Volumetric Flow Rate

Since the velocity profiles have been expressed in non-dimensional form, it is useful to do the same for the flow rate, so that:

$$Q = \frac{1}{\theta^2}\left\{\int_0^{\lambda_p} U_s \xi d\xi + \int_{\lambda_p}^{\lambda} U_c \xi d\xi + \int_{\lambda}^{1} U_p \xi d\xi\right\} \tag{58}$$

Where the dimensionless flow rate Q is introduced. As the purpose of the analysis is to eliminate the pressure gradient, τ_y is used to non-dimensionalize Q:

$$Q = q\left(\frac{\eta}{2\pi\tau_y R^3}\right) \tag{59}$$

It is clear by observation that the approximate ϵ term in the velocity profiles of Eq. 47 can now be set to zero as before, thereby precisely modelling the original shear distribution. Substituting in the velocity profiles from Eq.47 with $\epsilon = 0$ gives:

$$Q = \frac{1}{2\theta^2}\left\{\frac{\theta^2}{3}\left[\lambda^3 - \lambda_p^3\right] - \frac{2\theta}{7}\left[\lambda^{\frac{7}{2}} - \lambda_p^{\frac{7}{2}}\right] + \frac{1}{16}\left[\lambda^4 - \lambda_p^4\right] + \frac{\alpha}{16}\left[1 - \lambda^4\right]\right\} \tag{60}$$

However, the plug-flow boundary is also a function of θ, and can therefore be substituted into the above expression, again with $\epsilon = 0$:

$$\frac{\theta^2}{3}\left(3Q - \lambda^3\right) - \frac{2\theta}{7}\left(-\lambda^{\frac{7}{2}}\right) + \frac{1}{16}\left(-\lambda^4\right) + \frac{\alpha}{16}\left(1 - \lambda^4\right) + \theta^8\left(\frac{1552}{21}\right) = 0 \tag{61}$$

Now, for any constant value of Q, θ can be solved. Since the expression is an 8th order polynomial, it is not possible to solve analytically. The solution for θ can be substituted into the shear energy equation to give:

$$\dot{\Sigma}_s = \frac{1}{4\theta^4}\left\{\frac{\theta^2}{3}\left[\lambda^3 - \lambda_p^3\right] - \frac{2\theta}{7}\left[\lambda^{\frac{7}{2}} - \lambda_p^{\frac{7}{2}}\right] + \frac{1}{16}\left[\lambda^4 - \lambda_p^4\right] + \frac{\alpha}{16}\left[1 - \lambda^4\right]\right\} \tag{62}$$

Combining Eqs. 60 and 62 gives a simple relationship:

$$\frac{\dot{\Sigma}_s}{Q} = \frac{1}{2\theta^2} \tag{63}$$

Using Matlab, Equations 61 and 63 are solved for λ numerically over a range of α and Q. The algorithm used deduces λ based on selecting local minima in the shear energy profiles, so the validity of the solutions is certain.

Figure 13a shows the effect of varying the viscosity ratio α for $Q = 1$. As previously, the model predicts the thickness of the core layer to decrease with increasing viscosity. However, the influence on the viscosity ratio is stronger than in previous analyses, with the solution for λ lying at the vessel wall for $\alpha < 3.5$. Figure 13b shows the effect of varying flow rate for $\alpha = 4$. It can be seen that λ tends towards the centre

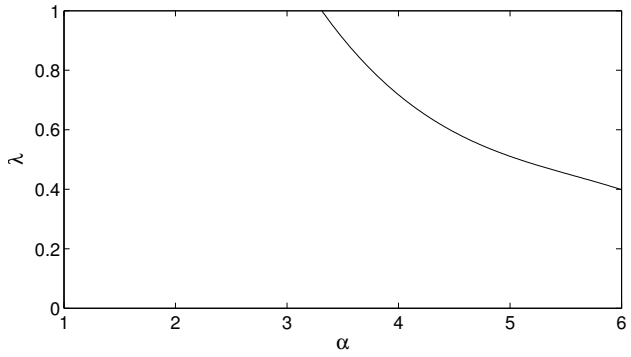

(a) Plot showing the effect of α on λ, $Q = 1$.

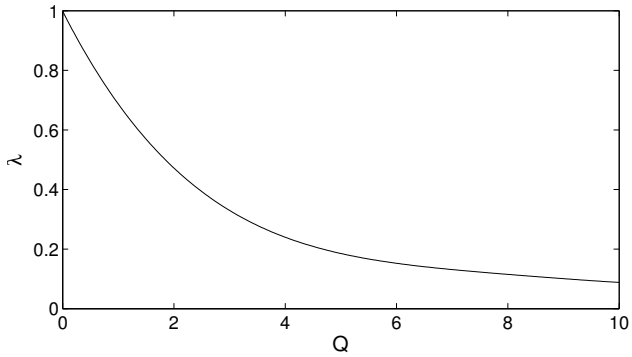

(b) Influence of Q on λ, $Q = 0 - 10$.

Figure 13

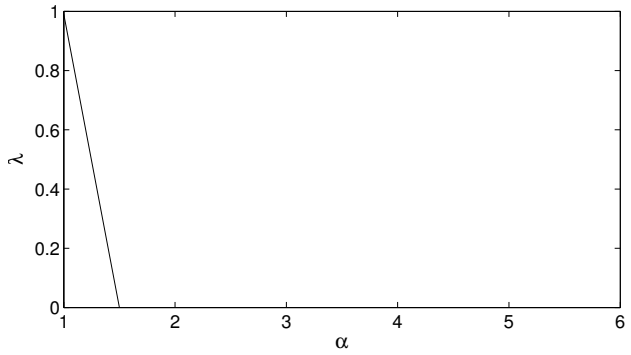

(a) Relationship between α and λ for $Q = 500$.

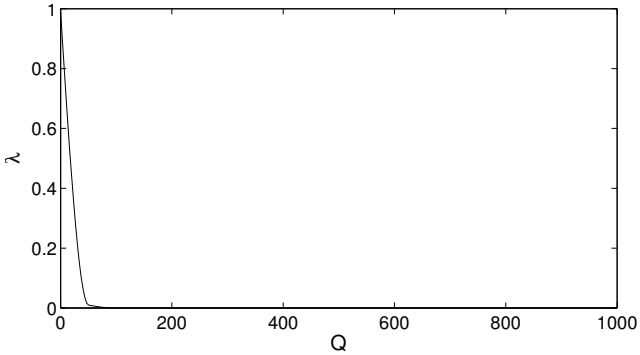

(b) Relationship between Q and λ for $Q = 0 - 1000$, $\alpha = 4$.

Figure 14

of the vessel as the flow rate increases, and so the $\frac{1}{R^3}$ term present in Eq. 59 suggests that small R values would cause the core layer thickness to decrease.

It is clear that under specific conditions, the model is able to predict physically realistic predictions for λ. However, the value of $Q = 1$ proves not to be a typical magnitude in the context of physiological flows. It is is possible to deduce from *in vivo* data provided by Bugliarello and Sevilla in Table 1 that typical total flow rates vary in the range $Q \approx 10 - 1000$. Figure 14a shows that at $Q = 500$, the flow has tended to a uniform composition, and that the two-phase separation is no longer prominent. Figure 14b confirms this observation, showing that λ tends to the vessel centre for $Q > 50$. The model thus has limited further applicability for blood flow, as was found with previous analysis for constant total flow rates.

3.3.2 Constant Core Flow Rate

The core flow rate is given by integrating the velocity distribution over the core layer as:

$$Q_c = \frac{1}{2\theta}\left\{\frac{\theta^2}{3}\left[\lambda^3 - \lambda_p^3\right] - \frac{2\theta}{7}\left[\lambda^{\frac{2}{7}} - \lambda_p^{\frac{2}{7}}\right] + \frac{1}{8}\left[\lambda^4\left(\alpha - \frac{1}{2}\right) - \alpha\lambda^2\right] + \frac{\lambda_p^4}{16}\right\} \tag{64}$$

where $Q_c = q_c\left(\frac{\eta}{2\pi R^3 \tau_y}\right)$. Substituting in the expression derived earlier for λ_p gives:

$$\frac{\theta^2}{3}\left[\lambda^3 - 3Q_c\right] - \frac{2\theta}{7}\left[\lambda^{\frac{7}{2}}\right] + \frac{1}{16}\left[\lambda^4 - 2\alpha\left(\lambda^4 - \lambda^2\right)\right] - \theta^8\left[\frac{1552}{21}\right] = 0 \tag{65}$$

The expression for the shear energy dissipation is identical to that in the case for constant total flow rate. Substituting for the pressure gradient in Eq. 62 gives:

$$\dot{\Sigma}_s = \frac{1}{2\theta^2} + \frac{\alpha}{32\theta^4}\left(1 + \lambda^4 - \lambda^2\right) \tag{66}$$

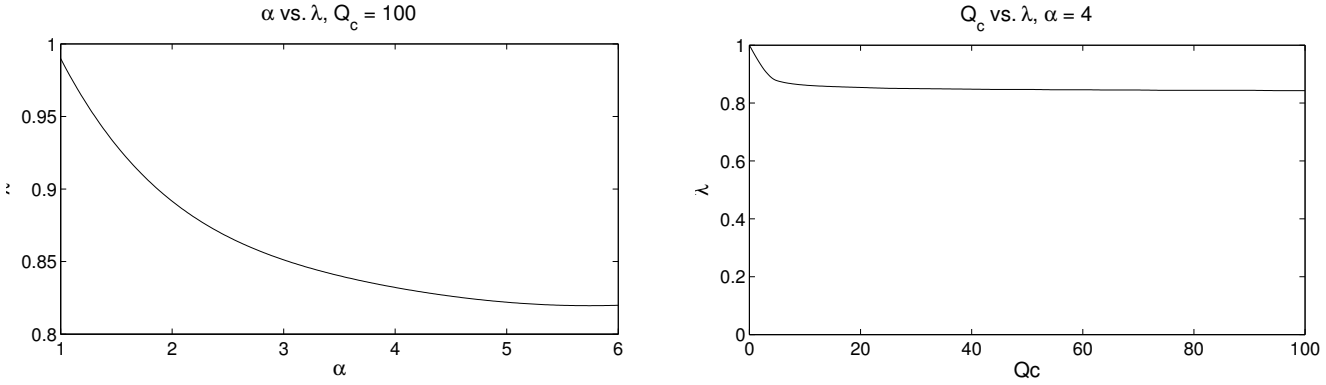

(a) Relationship between α and λ.

(b) Relationship between Q_c and λ.

Figure 15

Solving Eq. 65 numerically and substituting into Eq. 66, for a range of $\alpha = 1:6$ with a physically realistic value of $Q_c = 100$ taken from Table 1 gives the results shown in Fig. 15a after minimisation with respect to λ. In comparison to the analysis for a constant volume flow rate, the values of λ are less dependent on α and appear to tend to a constant value at approximately $\xi = 0.82$ as Q_c increases. This result is promising, as the solution remains physically valid over a larger range of core flow rates than for the case of a constant total flow rate.

Keeping α constant and varying Q_c gives the results shown in Fig. 15b. Again, the variation in λ with Q_c

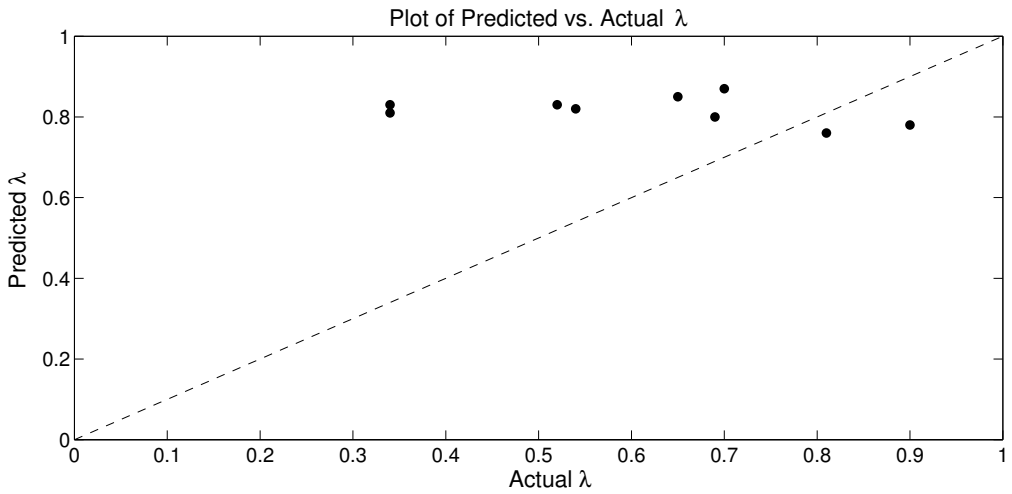

Figure 16: Comparison of model predictions to experimental data from Bugliarello and Sevilla.

is far less significant than the equivalent case with a constant total flow rate, emphasizing the behaviour shown at varying α.

Figure 16 shows a comparison between the values of λ predicted by the model to the experimental values obtained, with matched conditions. It can be seen that whilst the predicted values are all physically valid, they do not show a strong correlation to the experimental data. The variation in λ is found to be small as a consequence of the relatively large Q_c values.

3.4 Summary

A novel model has been proposed, capable of predicting the location of the separation boundary in a two-phase flow of blood, based on the minimisation of shear energy dissipation in a given fluid model. Three types of fluid have been considered, and in each case it was found that no solution exists for the case of a given pressure gradient, suggesting that this condition is not relevant in the context of the flows under study.

Consequently, it was considered that for physiological reasons, the flow might adopt a formation that would minimise the shear dissipation whilst providing a constant total flow rate. However, only in the case of a Casson fluid was a non-trivial solution found.

Lastly, it was proposed that if the main function of the blood supply were to provide a constant mass flow rate of erythrocytes, it could be the core flow rate that would be optimized. It was found that in all three fluid models a physically valid minimum of shear dissipation was found. The results show initial promise, confirming the trend of decreased core thickness with increased core viscosity observed experimentally.

However, neither the Newtonian nor general power-law fluid models demonstrated dependence on the vessel radius R and so could neither be matched with experimental conditions, nor provide a method of explaining the Fåhraeus–Lindqvist effect.

The Casson model was further developed with an intrinsic shear dependence making it amenable to comparison with available data. However, the results did not show good correlation with the data, varying only incrementally over the range of conditions under study.

4 Force Balance Model

4.1 Lift Forces Affecting the Particles

For a suspended particle in a non uniform velocity distribution, it can be shown that an angular velocity will be induced due to the differential velocity acting over the diameter of the particle. This angular velocity is given simply by the local velocity gradient, and the Kutta-Joukowski theorem states that the lift exerted on a body by an ideal fluid is equal to the product of the fluid density, the velocity of the body relative to the fluid flow and the fluid circulation about the body. By itself, this force will either cause a centripetal or centrifugal force due to the constant polarity of the velocity gradient over the vessel, and can therefore not explain the annulus effect. However, the observation that the suspended particles experience a velocity lag relative to the plasma adds additional complexity to the fluid behaviour, as will be discussed in the following analysis. Rubinow and Keller [27] showed that for a spinning sphere moving in a viscous fluid, the lift force imparted by the fluid can be given by:

$$f_L = \pi a^3 \rho_f \boldsymbol{\omega} \times \boldsymbol{u_{diff}} \tag{67}$$

where a is the sphere radius, ρ_f the fluid density, ω the angular velocity of the particle and u_{diff} its velocity relative to the fluid.

4.2 Diffusive Forces

Under the action of this lift force, each particle will tend to an equilibrium position. However, since there is currently no interaction between the particles, it is clear that all the erythrocytes would tend to aggregate at the same radial location, being driven either centripetally or centrifugally depending on the local differential velocity gradient. In reality, it is clear that this cannot occur, as the particles are of finite size. Therefore, in addition to the lift forces, there is likely to be a diffusive force that also acts dispersively upon the particles

proportional to their haematocrit gradient.

It is reasonable to assume that due to the scale of the particles in consideration, forces might exist akin to those known to act on dissolved chemical species. Considering such micro-particles, it is clear that in absence of any external forces the particles would tend to an equilibrium uniform distribution due to to Brownian motion, observed originally in pollen particles of a greater mass than that of an erythrocyte. It has also been suggested by Soo [28] that repulsive forces might arise from inter-particle collisions.

Before investigating further the detailed calculation of such a coefficient, it is useful to ascertain whether such a balance of forces could in theory lead to the particle distributions in question. The following section will begin by considering the application of these forces to the Newtonian fluid model.

4.3 Force Equilibrium in a Newtonian Fluid

The lift force per particle is given by Eq. 67. Therefore, for an elemental volume containing a volumetric fraction of particles H, the force acting on such an element would be:

$$F_L = \frac{H f_L}{V_{RBC}} = H \left(\frac{\pi a^3 \rho_f}{V_{RBC}} \right) \omega \times u_{diff} \tag{68}$$

where V_{RBC} denotes the volume of one erythrocyte. The angular velocity ω can be obtained as the derivative of the velocity profile, which in a Newtonian fluid is given as:

$$\omega = \frac{\partial}{\partial r} \left(1 - \frac{r^2}{R^2} \right) u_m = \frac{-r}{R^2} u_m \tag{69}$$

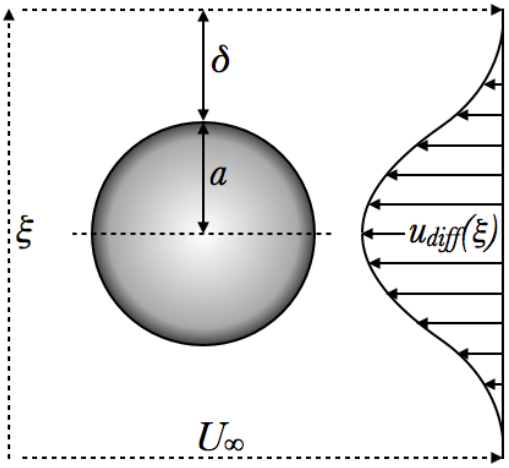

Figure 17: The disturbance factor δ.

where u_m is the centreline velocity. Next, an expression is needed for the differential velocity u_{diff}. One such expression is given by Goldsmith and Mason [29], obtained empirically as:

$$u_{diff} = \frac{2}{3} \left(\frac{a}{R} \right)^2 u_m \left[A \left(\frac{r}{R} \right)^4 + B \left(\frac{r}{R} \right)^2 + C \right] - \frac{u_m}{2} \left(\frac{a+\delta}{R} \right)^2 \tag{70}$$

where the constants $A = 3.04$, $B = 1.58$ and $C = 1.00$ were defined empirically by Mason [30] according to experimental data. Goldsmith and Mason [29] note that the moving spheres will cause a local flow disturbance in the surrounding fluid, so that its velocity will not be uniform. In order therefore to compute

u_{diff}, it is necessary to define an average local velocity. For this purpose, they include the term:

$$-\frac{u_m}{2}\left(\frac{a+\delta}{R}\right)^2 \tag{71}$$

where δ represents the flow disturbance factor, a distance past the radius of the erythrocyte to which the velocity of the surrounding flow is influenced, as illustrated in Fig. 17. Mason [30] found that the value of δ to which the experimental data best correlated was $\delta = \frac{a}{2}$, but also noted that the value of δ may affect the location of annulus formation, and may even be a function of $\xi = \frac{r}{R}$. However, at a first approximation, δ will be assumed here to be a constant value of $\delta = \frac{a}{2}$, as suggested by Mason [30]. The lift force per unit volume can then be expressed in full as:

$$F_L = H\left(\frac{\pi a^3 \rho_f u_m^2}{V_{RBC} R}\right)\left(-\xi\frac{2}{3}Z_0^2\left[A\xi^4 + B\xi^2 + C\right] - D\right) \tag{72}$$

Where $Z_0 = \frac{a}{R}$ the radial particle-vessel ratio and $D = \left(\frac{a+\delta}{\sqrt{2}R}\right)^2 = \frac{9}{8}Z_0^2$, the flow disturbance factor. The particles are assumed to rotate about an axis perpendicular to the direction of the flow, so the cross-product becomes a simple multiplication. As noted, according to Mason [30] D may affect the location of annulus formation, but here it can be seen that $Z_0\,(R)$ term is common to all contributing terms, and so here D is not independently a function of radius. Finally, the lift force must be in equilibrium with the diffusive force, which is assumed here to be proportional to the local haematocrit gradient, yielding:

$$F_D = -K\frac{\partial H}{\partial \xi} \tag{73}$$

where K denotes the unknown mass diffusion coefficient. Summing the two forces in Eqs. 72 and 73 gives:

$$\frac{\partial H}{\partial \xi} = H\left(\frac{\pi a^3 \rho_f u_m^2}{V_{RBC} RK}\right)\left(-\xi\frac{2}{3}Z_0^2\left[A\xi^4 + B\xi^2 + C\right] - D\right) = \Psi H\left(-\xi\frac{2}{3}Z_0^2\left[A\xi^4 + B\xi^2 + C\right] - D\right)$$

where $\Psi = \frac{\pi a^3 \rho_f u_m^2}{V_{RBC} RK}$, a dimensionless constant. Integrating the above expression gives:

$$H = \exp\left(-\frac{2}{3}\Psi Z_0^2\left(\frac{A}{6}\xi^6 + \frac{B}{4}\xi^4 + \frac{C}{2}\xi^2\right)\right)\exp\left(\frac{D\Psi}{2}\xi^2\right)\exp\left(\beta\right)$$

Where β is a constant of integration. The average value of the local haematocrit $H\,(\xi)$ across the vessel

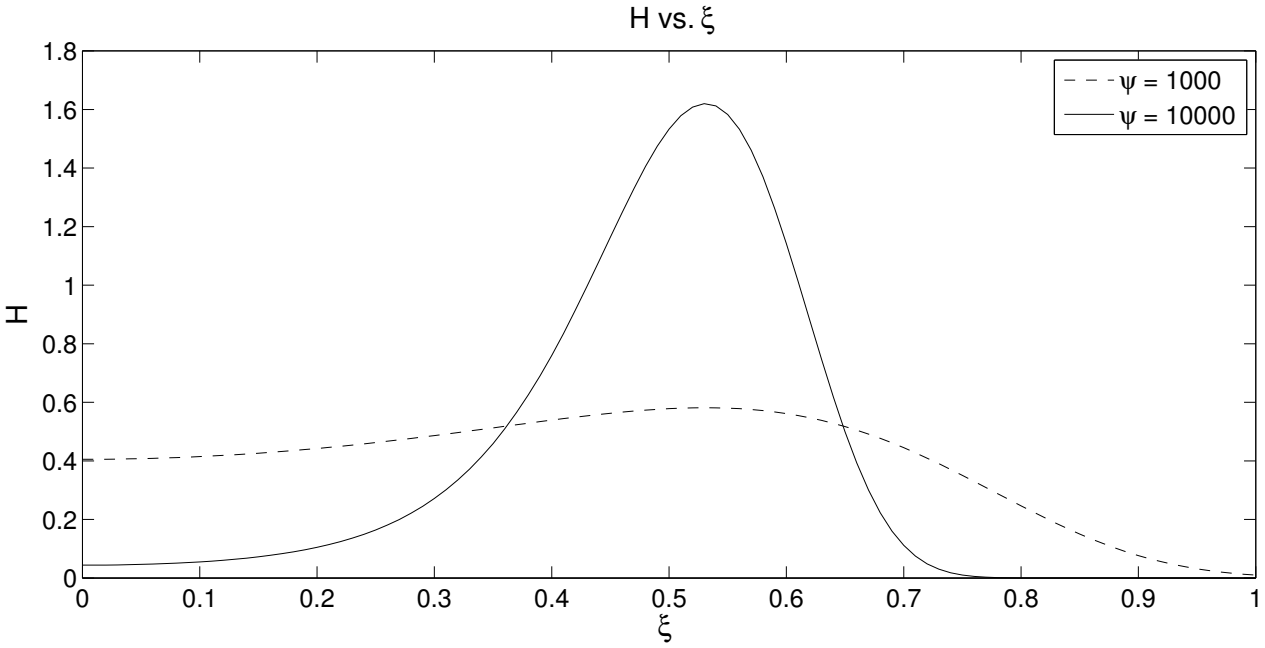

Figure 18: $H\left(\xi\right)$vs. ξ for Ψ=1000,10000.

must be equal to the tube haematocrit H_T. This can be expressed as the integral constraint:

$$\int_0^1 H d\xi = H_T \tag{74}$$

It is not possible however to integrate analytically a function of the form $f\left(x\right) = e^{x^n}$, so the above constraint must be applied numerically. Solving $H\left(\xi\right)$ across the vessel for varying values of Ψ gives the results shown in Fig. 18.

Promisingly, the model can be seen to predict both the annular and cell-rich core types of behaviour observed by Segré and Silberberg [3], with the behaviour being strongly dependent on the constant Ψ. Comparing Fig. 18 to the observed effects in Fig. 5, the formation of the annulus at $\xi \approx 0.53$ is evident. However, it is the second plot corresponding to $\Psi = 1000$ that is of predominant interest to this investigation, as it appears to show clearly a large concentration of particles at the centre of the vessel, mimicking a two-phase separation. Although the diminishing local haematocrit towards the vessel wall is perhaps not steep enough to be identified as a definite phase boundary, it is reasonable to suppose that an approximate value of λ could be obtained from such a distribution.

Whilst the results of this initial analysis are encouraging, it is important to note that assuming the diffusive force to be proportional to the local haematocrit gradient is only applicable in the case of one dimensional diffusion.

4.3.1 Force Equilibrium in Cylindrical Sections

The local haematocrit gradient in a curved vessel differs to that in a one-dimensional cross-section, which is illustrated by balancing forces on the cylindrical element in Fig. 19. Assuming that a pressure acts on the element proportional to the local haematocrit, the net force can be calculated as:

$$F_D = K\frac{\left\{\left(H+\frac{\partial H}{\partial r}\delta r\right)\left(\delta\theta\left(\frac{r+\delta r}{r}\right)\right)-\left(H\delta\theta\left(\frac{r}{r}\right)\right)\right\}}{\delta r} \tag{75}$$

which, ignoring higher order terms yields:

$$F_D = \frac{K}{r}\frac{\partial\left(Hr\right)}{\partial r} = \frac{K}{\xi R}\frac{\partial\left(H\xi\right)}{\partial\xi} \tag{76}$$

which contrasts with the assumption for the case of a one-dimensional section. The lift force remains the same in the case of a cylinder, as it is not a function of the vessel geometry. Proceeding therefore in the same manner, equating the lift and diffusive forces gives:

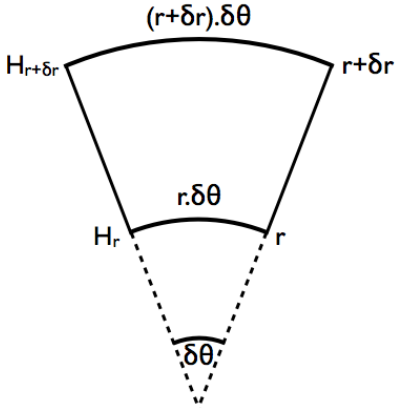

Figure 19: An element of cylindrical area.

$$\frac{\partial H}{\partial\xi} = H\left[f_L\frac{R}{K}-\frac{1}{\xi}\right] \tag{77}$$

By inspection, it is evident that analytically the integration of this function over the entire vessel presents a problem at the centre, where the function tends to infinity as the denominator tends to zero. Physically this is an impossibility, as the local haematocrit cannot exceed $H\left(\xi\right)=1$. The integration is therefore carried out between an, as yet unknown boundary ξ_b, at which the concentration is assumed to have a value H_b:

$$\frac{H}{H_b} = \exp\left\{-\frac{2}{3}\Psi Z_0^2\left[\frac{A}{6}\left(\xi^6-\xi_b^6\right)+\frac{B}{4}\left(\xi^4-\xi_b^4\right)+\frac{C}{2}\left(\xi^2-\xi_b^2\right)\right]\right\}\exp\left\{\frac{\Psi D}{2}\left(\xi^2-\xi_b^2\right)\right\}\frac{\xi_b}{\xi} \tag{78}$$

As a boundary condition must be specified, the boundary concentration is set arbitrarily to $H_b=0.4$ here as a first approximation. The value H_b is taken to be the point at which the gradient of the velocity profile $\frac{\partial u}{\partial\xi}=0$, and can be obtained from the numerical solution of:

$$A\xi^3+B\xi^2+\left(C-\frac{3}{2}\frac{D}{Z_0^2}\right)\xi+\frac{3}{2}\frac{1}{\Psi Z_o^2}=0 \tag{79}$$

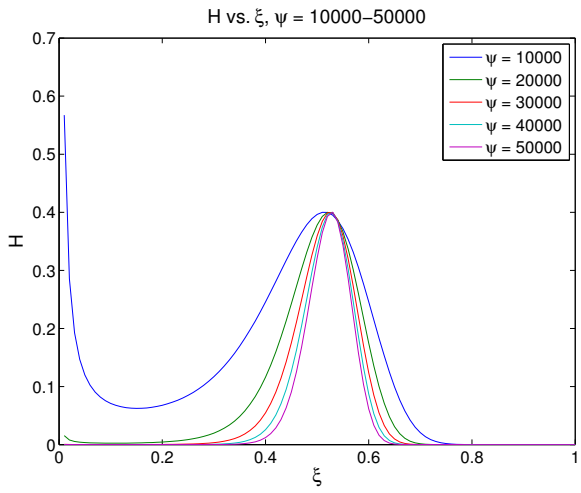

(a) Plot showing the effect of Ψ on H.

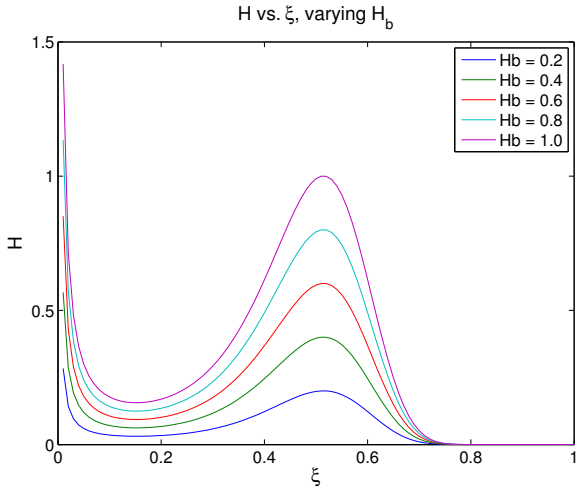

(b) Plot showing the effect of H_b on H.

Figure 20

The initial value of this boundary concentration has an effect on the magnitude of the distribution produced, but not the shape as can be seen in Fig. 20b. Therefore, the value of H_b does not affect the position of the annulus, and so the arbitrary setting of H_b does not affect the analysis.

4.3.2 Effect of R

Fig. 21a shows the effect of varying the vessel radius R on the plots. As was discovered in the previous chapter in the study of the energy minimisation, the value of R has no significant effect on the position of the annulus formation, but a similar effect to the constant Ψ on its shape and magnitude. This behaviour can be confirmed by examination of Eq. 78, all the terms are equal functions of $Z_0(R)$, and therefore R does not affect the proportional contributions of the individual terms, only the overall magnitude of the distribution.

4.3.3 Effect of δ

Mason [30] proposed that it is possible that the value of $\frac{\delta}{a}$ may have an effect on the position of the annulus formation, but no quantitive investigation was undertaken. Referring again to Fig. 17, an average fluid velocity u_{af} can be computed, leading to the differential velocity $U_{diff} = u_p - u_{af}$ that is crucial in producing the differential velocity gradient responsible for the observed effects.

It can be clearly seen in Fig. 21b that the position of the annulus formation is significantly affected by the choice of $\frac{\delta}{a}$, and it can be shown that varying the magnitudes of the constants A, B and C has a

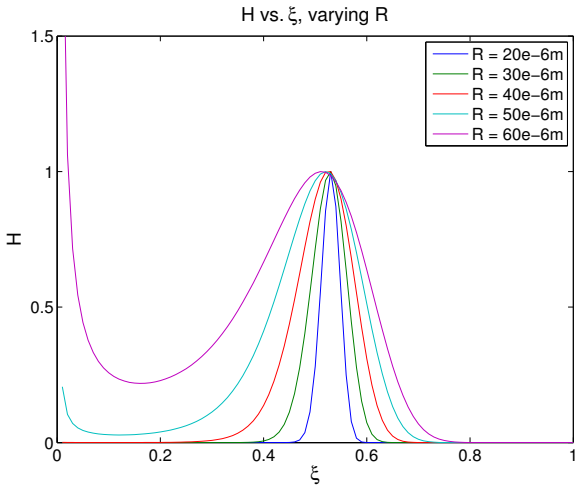

(a) Plot showing the effect of R on H.

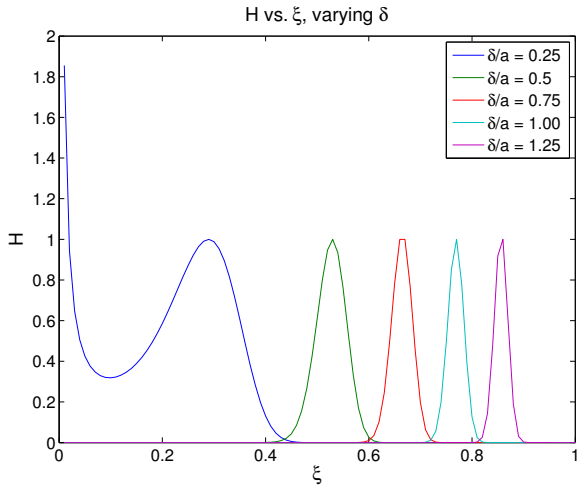

(b) Plot showing the effect of $\frac{\delta}{a}$ on H.

Figure 21

similar effect[1], however these constants are not considered variable by Goldsmith and Mason [29], and are not further considered. From Eq. 70, it can be seen that the value of $\frac{\delta}{a}$ will affect the magnitude and, more importantly, position of contraflexure of u_{diff}, as is seen in Fig. 22. Setting $u_{diff} = 0$ and $\xi = 0$ in Eq. 70, it can be calculated that for $\frac{\delta}{a} = 0.1547$, the differential velocity is positive over the range of the vessel, imparting positive angular velocity and therefore an inwardly directed force towards the centre of the vessel. Increasing δ shifts the profile so that the velocity distribution crosses the $u_{diff} = 0$ axis as can be seen in Fig. 22, creating a point of contraflexure at a position along the vessel radius. This distribution will impart a positive force on cells in the centre, causing outward migration, and a negative force on cells near the wall, causing inward migration. Consequently, the cells will tend to aggregate at the point of contraflexure causing the annulus effect observed, as argued by Repetti and Leonard [23]. The point of annulus formation pushes further towards the wall until $\frac{\delta}{a} = 1.737$, this being calculated in a similar fashion, at which point the velocity gradient is negative across the vessel radius and all cells are propelled towards the outer wall.

4.3.4 Effect of Psi

The range of concentration distributions illustrated in Fig. 24 can be explained through consideration of Eq. 78. While it is known that the equation comprises both lift and diffusive force components, it is observable by inspection that whilst Ψ is present as an exponent throughout the equation, the polarity of the exponent varies, and so varying the value of Ψ therefore varies the relative magnitudes of these

[1] Results not shown here.

contributing elements. It is useful to consider the behaviour of the two forces independently to assess the oberved behaviour further.

In absence of a diffusive force, the lift force would act so as to concentrate the erythrocytes at an infinitely sharp peak at the point where the velocity gradient equals zero, as proposed by Repetti and Leonard [23]. Conversely, the diffusive force will adopt an equilibrium distribution in absence of the lift force, which can be obtained by the solution of $\frac{\partial(rH)}{\partial r} = 0$. The resulting equilibrium distribution is of the form $H = \frac{A}{r}$ where as a result, the erythrocytes will tend to an infinite concentration at the centre of the vessel, which is not physically realistic.

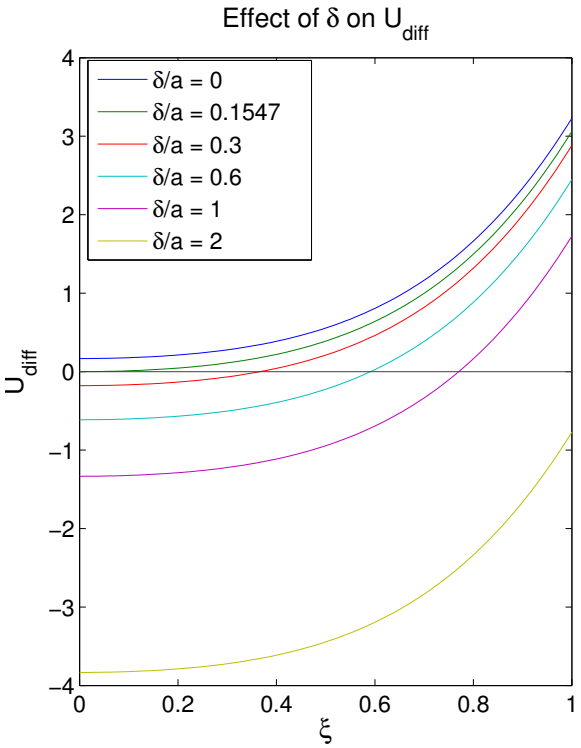

Figure 22: Plot showing the effect of $\frac{\delta}{a}$ on u_{diff}.

It is thus possible to interpret the distributions clearly. For small values of Ψ, the solution exhibits the central peak characteristic of what might be expected from pure diffusion, with a negligible contribution by the lift force. As Ψ increases, the relative magnitude of the lift component increases until at approximately $\Psi \approx 10000$ the two forces are effectively balanced, exhibiting a cell-rich core. Increasing Ψ further increases the effect of lift, until the diffusive contribution becomes negligible so that the solution exhibits a singular peak of diminishing width, characteristic of what might be expected in the absence of diffusion.

Solving the concentration distribution to the centre of the vessel, it is interesting to observe that the solution does not tend to infinity for all values of Ψ. As can be seen in Fig. 20a, for values of $\Psi \gtrsim 20000$ the concentration drops to zero towards the centre. Fig. 24 shows the solution at a wider range of Ψ, showing that both the characteristic annular and cell-rich core formations are produced in different parameter ranges.

4.3.5 Results and Discussion

The shape of the concentration distribution has been demonstrated to be strongly dependent on Ψ. Whilst the annulus shape observed exhibits two points of contraflexure where $\frac{\partial H}{\partial \xi} = 0$, at larger values of Ψ the

local haematocrit tends monotonically to infinity at the vessel centre, with no points of contraflexure within the vessel boundary. Therefore, it can be assumed that at some limiting value of Ψ there will be a single point of contraflexure between these two states where the concentration will plateau, resembling the cell-rich core sought by this investigation. This can be observed in Fig. 23a, where the limiting value of Ψ is calculated as $\Psi \approx 2616.85$, where there exists only one solution for $\frac{\partial H}{\partial \xi} = 0$. It is interesting to observe that even in this case, the concentration still tends to infinity at the centre, as shown in Fig. 23b.

The infinite spike is a consequence of the singularity existing at the centre of the cylinder, where the elemental volume tends to zero and the concentration is then by definition $\frac{NV_{RBC}}{0} = \infty$. In theory, it might be possible to overcome this problem by implementing the diffusion coefficient as a function of $K(H)$, so that for values of $H > 1$ the repulsive force would be infinite, as would be physically realistic if considering a particle of finite volume. It is apparent after investigation however that this approach is not valid due to equilibrium diffusive distribution being independent of the diffusion coefficient K.

In order to compare meaningfully the validity of this model, it is necessary to compare the results with the experimental data in Table 1, and to do so a consistent method of determining λ from the concentration distributions is required, and proposed as follows.

Firstly, the value of Ψ must be adjusted so that the characteristic cell-rich core distribution is exhibited, and only one point of contraflexure $\frac{\partial H}{\partial r} = 0$ exists at $\xi = \xi_b$. The infinite spike can be ignored, as it is physically unrealistic. As Ψ is a function of the physical parameters of the flow, it would then be possible to determine the value of the diffusion coefficient K after matching all other conditions with experimental data. If the model is realistic and there does indeed exist a diffusive force behaving as proposed, the value of K should remain constant for the range of flows.

Secondly, the boundary position λ is determined, and can by being assumed to occur approximately at the drop off of the annulus formation. However, this definition introduces a problem in that that apart from small variations resulting from the gradient of the annulus drop-off, the position of λ will clearly not vary considerably with Ψ, and will not therefore compare meaningfully with the experimental data.

The position of this annulus has however been demonstrated to vary considerably with the flow disturbance factor $\frac{\delta}{a}$, which has been considered as constant according to Goldsmith and Mason [29]. If correct, this model suggests that, whilst the combination of forces is important in producing the characteristic distribution, it is in fact $\frac{\delta}{a}$ that is the important parameter in determining the position of λ. However, there currently exists no method of relating this parameter to the flow conditions, as it has so far only been measured experimentally under particular conditions.

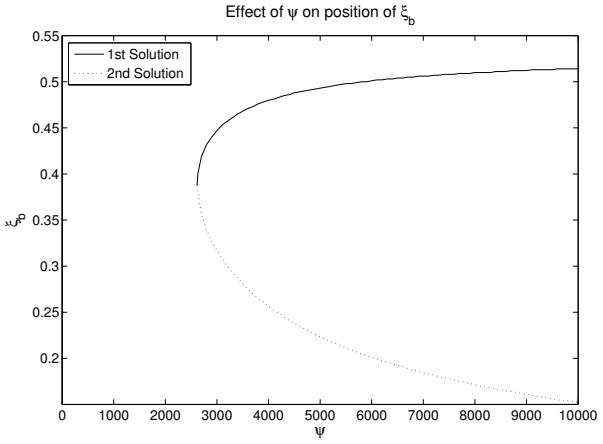

(a) Plot showing the effect of Ψ on both solutions for ξ_b.

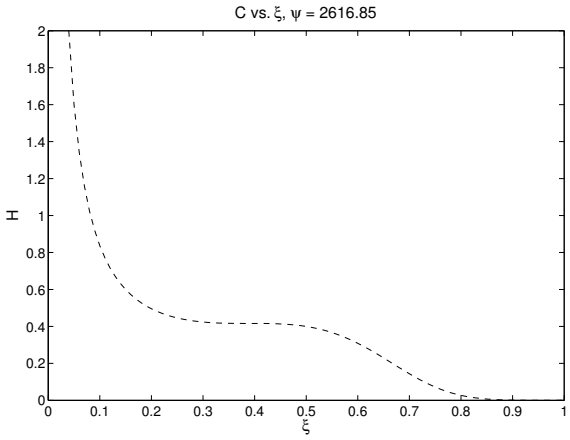

(b) Plot showing C vs. ξ for the case of limiting Ψ.

Figure 23

A method of determining the particle lag was attempted by equating the Stokes' Drag [31] $F_D = 6\pi\mu a u_{diff}$ to a momentum deficit $D = \int_{\infty}^{\infty} u_f \left(u_\infty - u_f\right)$. Ultimately however, this approach was not pursued further as it would have necessitated a sweeping assumption of the form of the fluid velocity distribution u_f within the flow volume, leading to further complications.

The disturbance factor is a complex one, as the extent of this disturbance will likely be highly dependent on flow conditions and physical parameters. In addition, the task of computing simultaneously the interaction of multiple flow fields means that its effective determination is unfortunately beyond the scope of analytical techniques. However, its importance as a factor affecting the boundary layer position would certainly make it worthy of detailed further analysis, through the use of computational fluid dynamics techniques, which were not feasible here given the timescale of the investigation.

In summary, the current model has been found to exhibit an infinite centre concentration, but not to produce a realistic variation in λ given the physical variables being considered. There is however merit in its ability to exhibit the desired cell-rich core flow phenomenon, and it is clear that the lift-diffusion model proposed has shown promise in this regard. It is possible however that these imperfections are due to the assumption of a Newtonian fluid.

The Casson fluid model has already been demonstrated to exhibit shear-dependent behaviour, and may produce a model to predict λ with more dependence on the physical parameters in question. Secondly, it is easy to perceive how a Casson fluid might eliminate the difficulty of an infinite core concentration, as in this case it would be possible to implement the plug-flow region more realistically. As noted previously, the plug-flow boundary occurs at the point where the velocity gradient equals zero, and within this region the

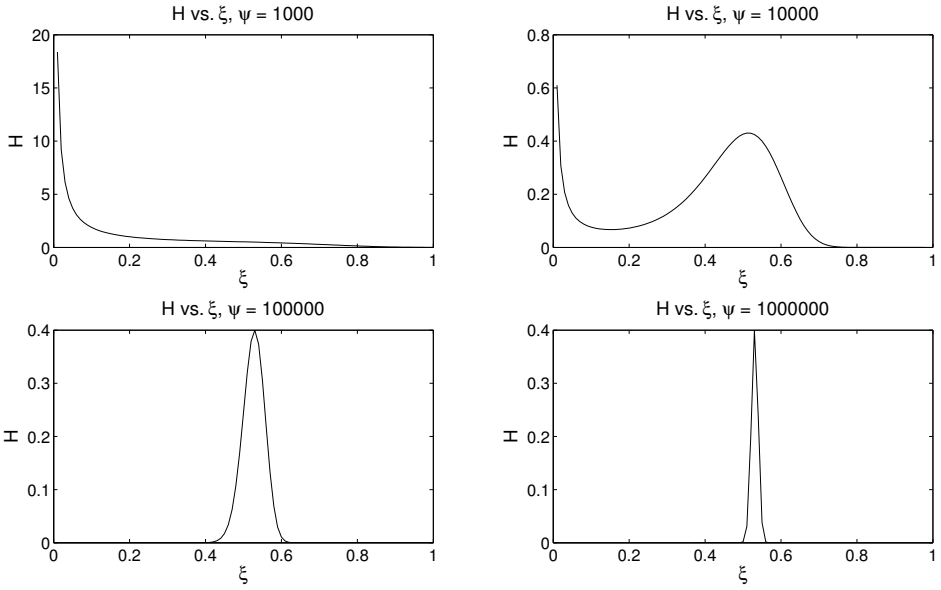

Figure 24: The effect of ψ on H.

velocity is constant. This zero velocity gradient would not impart any angular velocity on the erythrocytes, therefore no lift force would be acting upon them. In absence of this force, the cells should adopt a uniform equilibrium distribution, and the concentration within the plug-flow region a constant value, equal to that at the plug-flow boundary λ_b. The next section will therefore apply the force equilibrium model to a Casson fluid.

4.4 Force Equilibrium in a Casson Fluid

Firstly, the angular velocity imparted by the fluid flow on the cells must be calculated. The velocity gradient is obtained by rearranging the expression for the shear force and substituting in $\tau = \frac{-Pr}{2}$, yielding in non-dimensional form:

$$\Omega = \frac{\omega\eta}{PR} = -\left[\sqrt{2}\theta + \frac{1}{\sqrt{2}}\sqrt{\xi}\right]^2 \tag{80}$$

Substituting in Eq. 80 into Eq. 77 from the previous analysis gives:

$$\int_{H_p}^{H} \frac{1}{H} dH = \int_{\xi_p}^{\xi} \left(-\Psi \left[\sqrt{2}\theta + \frac{1}{\sqrt{2}}\sqrt{\xi}\right]^2 \left[\frac{2}{3} Z_0^2 \left(A\xi^4 + B\xi^2 + C\right) - D\right] - \frac{1}{\xi} \right) d\xi \tag{81}$$

However, the boundary λ_p is known from previous analysis as $\lambda_p = 4\theta^2$. The integration is therefore carried out over this range, and the concentration within the core region set to the value at the boundary, $H\left(\xi_p\right)$. The results of the analysis are shown for a range of values of Ψ in Fig. 25.

However, there are now two dimensionless variables that can affect the concentration, having reintro-

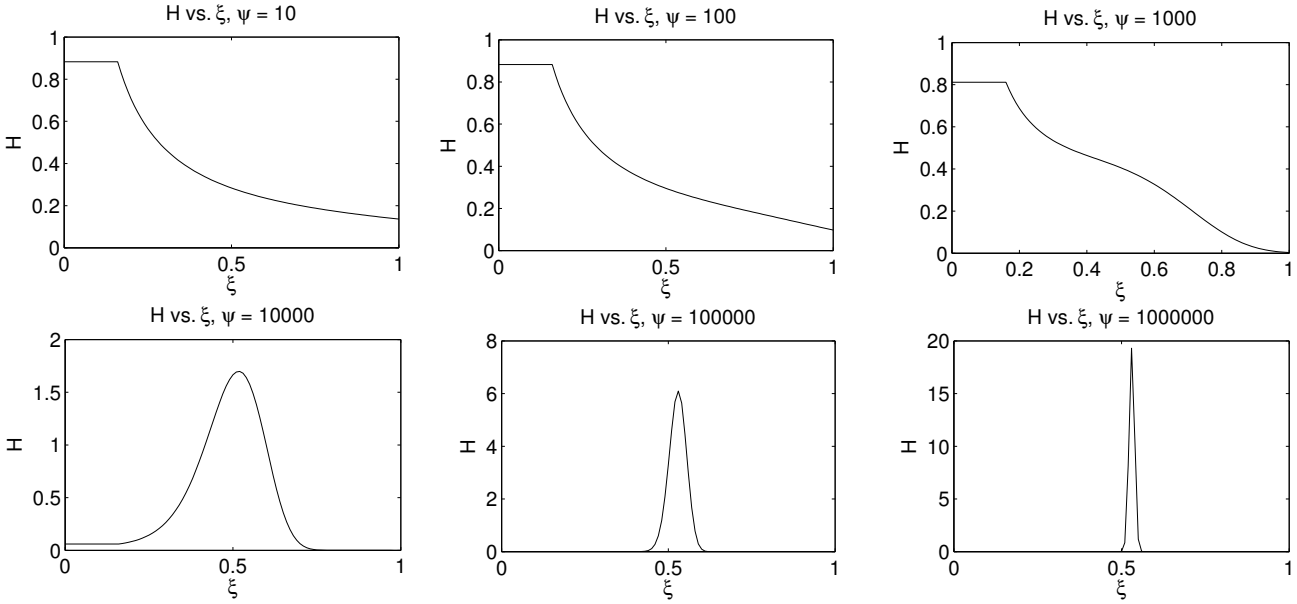

Figure 25: The effect of varying Ψ on H.

duced the dimensionless pressure gradient θ. Fig. 26 shows the effect of varying θ.

It can be seen from Fig. 25 that similar distributions are produced to those observed previously. Again, it can be concluded that those distributions of the annular form where the peak concentration surpasses unity are not physically valid representations. As stated, the solutions that are of most interest are those for which the concentration remains within the unity boundary. Fig. 26 demonstrates that the value of θ defines the plug flow boundary, as predicted by Eq. 49, however in the distributions sought it is not this boundary that defines λ, although the existence of this boundary does remove the infinite concentration at the vessel centre.

It is important to note that as a Casson fluid is now being considered, the parameters τ_y and η are both functions of haematocrit. Previously, these were assumed to adhere to the tube average haematocrit value, H_0, however it is more realistic to assume that their values vary with local haematocrit H. This indicates a second limitation of the previous model, in that it is assumed that the velocity distribution is independent of the haematocrit distribution. The velocity distribution is in fact a function of the parameters τ_y and η, and therefore of the concentration distribution. In order to maximise the accuracy of the model, it is necessary to solve for both the velocity and concentration distributions concurrently.

4.4.1 Casson Fluid With Integrated Parameters

For the purposes of comparison with experimental data, it is possible to substitute the unknown pressure gradient P for an expression in terms of the central velocity u_m, obtained by equating the velocity at the

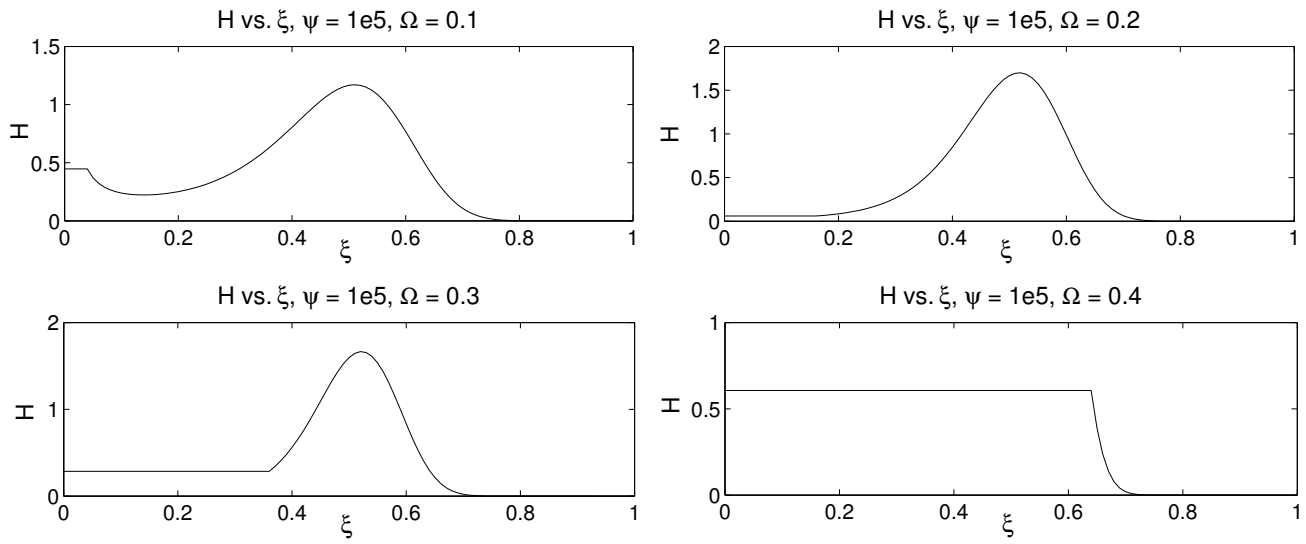

Figure 26: The effect of varying θ on H.

plug-flow boundary from Eq. 47 to u_m. The profile is in similar form to that in Section 3, only without the peripheral plasma layer. Integrating the Casson shear function and imposing the non-slip condition at the wall gives:

$$u\left(\xi\right)\frac{2\eta}{\tau_y R}=\frac{\left(1-\xi^2\right)}{4\theta^2}+\frac{4}{3}\frac{\left(1-\xi^{\frac{3}{2}}\right)}{\theta}+\left(1-\xi\right) \tag{82}$$

which at the location of the plug flow boundary $\lambda_p = 4\theta^2$ becomes:

$$u_m\left(\frac{2\eta}{\tau_y R}\right)=\frac{\left(1-16\theta^4\right)}{4\theta^2}+\frac{4}{3}\frac{\left(1-8\theta^3\right)}{\theta}+\left(1-4\theta^2\right) \tag{83}$$

The concentration gradient can be rearranged from the previous section as:

$$\int_{H_a}^{H}\frac{1}{H}dH=\int_{\xi_a}^{\xi}\left(\left\{-\Psi\left[\frac{2}{3}Z_0^2\left(A\xi^4+B\xi^2+C\right)-D\right]\frac{\tau_y\left(H\right)}{\eta\left(H\right)}\left[1+\frac{\sqrt{\xi}}{2\theta\left(H\right)}\right]^2\right\}-\frac{1}{\xi}\right)d\xi \tag{84}$$

where $\Psi=\frac{\pi a^3\rho_f u_m R}{V_{RBC}K}$, and θ can be solved numerically when defining u_m. Clearly, to account for the variation in the Casson parameters τ_y and η is problematic, as the plug flow boundary is no longer constant, but is a function of H. Similarly to the previous analysis, it is not possible to integrate over the vessel space without specifying a Dirichlet boundary condition, and so a point along the vessel denoted ξ_a must be assumed to take a specific value H_a. However, where before it would have been reasonable to take this point as the plug flow boundary for consistency, it is not now possible to determine the point at which

this occurs without first solving for the concentration profile. In addition, it is clear that the boundary value concentration H_a will affect the position of the plug flow boundary.

It was therefore necessary to adopt an iterative approach in determining the position of annulus formation ξ_a, repeatedly solving for the concentration profile from an assumed midpoint until that point aligned with ξ_a, confirmed by observing the radial shear variation. After solving for the correct concentration distribution, it was then possible to determine the position of the plug flow boundary by considering the shear variation.

4.5 Results and Discussion

Solving for the concentration distribution across the vessel, it is apparent that the value of Ψ plays a similar role to that seen previously, in that an increase in Ψ tends to force the erythrocytes away from the centre into a concentrated peak at $\lambda = 0.53$. This value of λ is found to be constant with variations in Ψ, following the behaviour observed earlier.

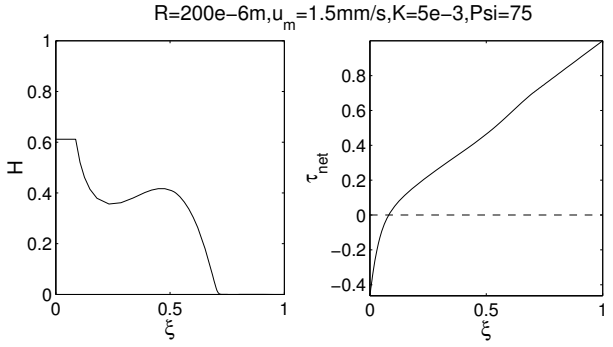

(a) Plot showing the effect of the shear distribution on H.

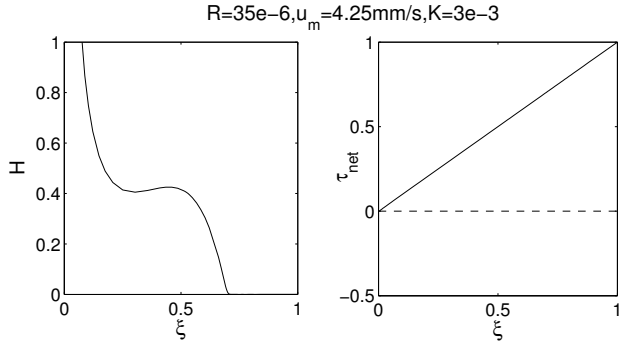

(b) Plot showing the effect of the shear distribution on H.

Figure 27

It therefore seems highly likely that the variation of Ψ by itself does not provide a mechanism by which to predict the location of the phase boundary. However, by integration of the Casson parameters $\tau_y\,(H)$ and $\eta\,(H)$, a link has been introduced between the value of Ψ and the plug flow boundary, governed by the dimensionless pressure gradient θ, which is now a function of the centreline velocity u_m. This constant velocity term also affects Ψ, as does the vessel radius R, both appearing in the numerator of $\Psi = \frac{\pi a^3 \rho_f u_m R}{V_{RBC} K}$. Conversely, they exist as a ratio $\frac{u_m}{R}$ in the expression for θ, and so the two parameters can be varied independently by altering the magnitudes of the two parameters proportionally.

In varying both u_m and R, it is found that the magnitude of the plug flow boundary is only of comparable order to that of the annulus position over a small range of conditions, and exists negligibly as $\lambda_p \approx 0$ when comparing with the data from Table 1, eliminating any possibility that the position of the plug flow boundary might denote the phase-boundary. Fig. 27b shows the model prediction corresponding to the data from row nine of Table 1, chosen so as to maximise the thickness of the plug flow region for demonstration. As can be observed, even in the most extreme of the experimental instances the plug flow region is negligible, with the net shear being positive over almost the entire vessel. However Fig. 27a demonstrates that in the case of slower velocities this effect does become prominent, illustrated as the point at which the net shear becomes negative. Fig. 28 shows the velocity profiles of the two solutions with the plug flow region coinciding with the shear variation.

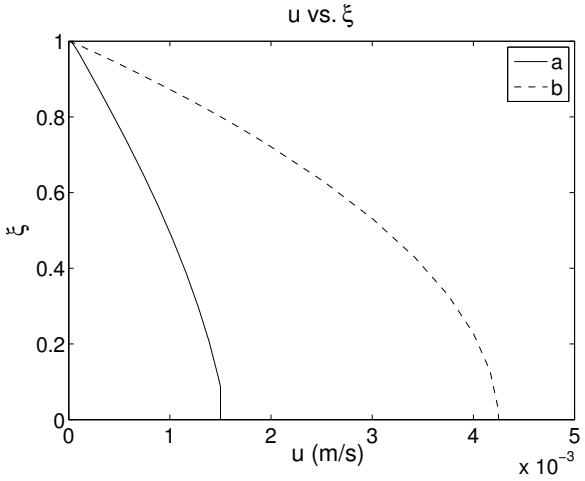

Figure 28: Velocity profiles a & b corresponding to Figs.27a & 27b respectively.

4.6 Summary

A model describing the distribution of erythrocytes in suspension has been proposed by analyzing the forces acting on individual particles. Both a lift force, resulting from particle rotation, and a diffusive force are proposed to act in conjunction.

The model shows good qualitative promise in reproducing observed concentration distributions, but does not provide a method for producing reliable quantitative estimates for the position of the phase boundary λ through the manipulation of the parameters under consideration.

It is found that the boundary position is invariant over a range of conditions, showing a consistent location of approximately $\lambda \approx 0.53$, shown to coincide with the point of contraflexure of the velocity distribution. Notably, it is demonstrated that whilst the particles may tend to aggregate about a point in the presence of the lift force, it is only with the novel addition of a diffusive force that the cell-rich core distributions can be achieved. The diffusive force coefficient K has not been determined as constant in achieving similar distributions under different conditions, but it remains plausible that such a parameter might be a function of these conditions, and so remains a promising hypothesis.

A semi-empirical model for the particle velocity lag has been implemented from the literature, assuming

the flow disturbance factor $\frac{\delta}{a}$ to be constant, but it is shown however that $\frac{\delta}{a}$ strongly influences the position of the phase boundary. Further attempts to deduce theoretically an expression for $\frac{\delta}{a}$ were not pursued due to the complex nature of the task, which would consider the complex interaction of numerous particle flow fields and likely require a numerical approach.

5 Conclusion

Before considering the mechanisms whereby a two-phase separation might be established, it is important to consider the physiological implications of such an arrangement. The 50-300μm diameter range encompasses the arterioles and venules, excluding the capillary domain and therefore no exchange of nutrients occurs, with the vessels functioning purely for transport. Considering this, it can in fact be demonstrated[2] that for a constant mass flow rate of erythrocytes, the diffusion from the vessel is in fact minimised at a radius of approximately $\lambda = 0.61$, corresponding to typical values observed experimentally by Segré and Silberberg [3], and the value $\lambda = 0.53$ predicted by the force model. It can therefore be reasoned that the phase separation occurs to conserve oxygen within the erythrocytes before reaching the capillaries, where it can be exchanged more efficiently.

It was shown in Section 3 that when considering a two-phase flow of blood subject to a constant core flow rate, with a Casson fluid core and Newtonian peripheral layer, there does exist a boundary location λ for which the rate of shear energy dissipation is minimised. However, whilst the model predictions are physically valid, they do not show strong agreement to experimental data, being only weakly dependent on the flow conditions. The model developed is extensive in its consideration of experimental conditions and fluid models. The inaccuracies in its predictions must therefore stem from a flaw in the underlying hypothesis, and it is consequently unlikely that microvascular flows are arranged to minimise shear energy dissipation.

Section 4 considered the particle distribution to be achieved by both a lift force due to particle rotation, and a diffusive force acting in conjunction. This novel model succeeds in reproducing complex particle distributions observed experimentally, that cannot be achieved by either of these forces acting independently. However, it is found that the separation boundary is strongly dependent on the flow disturbance factor δ, which is considered to be constant, and determined empirically. The force model shows promise as a potential mechanism for causing the two-phase flow, and should be investigated further to fully assess its merit.

[2] See Appendix

5.1 Future Work

It was not possible to fully explore every aspect of this investigation, and so the following avenues are left for future analysis:

- The shear energy minimisation should be applied fully to the two-phase flow of a power-law fluid, with different core and plasma dimensionless behaviour indices n.
- A mechanism for diffusion in the force model should be investigated more rigourously, and a quantitative expression for the diffusion coefficient K deduced.
- A theoretical expression for δ should be developed, and its dependence on the flow conditions investigated.
- This investigation approximated the erythrocytes as spheres, when they are in fact shaped as biconcave disks. It is possible that their geometry affects the flow, and so warrants exploration.

6 Appendix

In considering the primary role of the microvasculature, it would be reasonable to propose that the two-phase configuration might offer some benefit to the diffusion of nutrients and waste products between the surrounding cells. Considering a steady state haematocrit gradient, the following equation describing diffusion in a cylinder is obtained:

$$\frac{1}{r}\frac{\partial}{\partial r}\left(r\frac{\partial C}{\partial r}\right) = 0 \tag{85}$$

Integrating this expression, an equation for each of the two layers is obtained, denoting the local haematocrits at the boundary and the cell wall as H_b and H_w respectively:

$$H_b = A\ln(\lambda r) + B_b \qquad and \qquad H_w = \ln(R) + B_w \tag{86}$$

Solving these equation, the constants of integration A and B can be found as:

$$A = \frac{H_b - H_w}{\ln(\lambda)} \qquad and \qquad B = \frac{H_w \ln(\lambda R) - H_b \ln(R)}{\ln(R)} \tag{87}$$

Substituting into the integrated form of Eq. 85 yields:

$$H = \frac{H_b \ln(\xi) - H_w \ln\left(\frac{\xi}{\lambda}\right)}{\ln(\lambda)} \tag{88}$$

Next, the mass flux at the vessel wall is equated to that across the wall. Denoting the haematocrit in the cells outside the vessel H_c and introducing the membrane mass transfer coefficient h and diffusion coefficient D yields:

$$-D\frac{\partial H}{\partial r}(2\pi r)\bigg|_{r=R} = h(2\pi R)(H_w - H_c) \tag{89}$$

Substituting $\frac{\partial H}{\partial r} = \frac{A}{r} = \frac{1}{r}\frac{H_c - H_w}{ln(\lambda)}$ from Eq. 85 and rearranging gives:

$$\dot{M}_c = \frac{2\pi D(H_b - H_c)}{\frac{D}{hR} - \ln(\lambda)} = \frac{2\pi D(H_b - H_c)}{\frac{1}{Sh} - \ln(\lambda)} \tag{90}$$

where $\dot{M}_c$ denotes the mass transfer to the cells, and the Sherwood number, $Sh = \frac{hR}{D}$ represents the ratio of convective and diffusive mass transfer coefficients. The mass transfer to the cells will ultimately be limited by the mass supply provided by the blood flow, denoted $\dot{M}_s$. Assuming therefore that this nutrient supply is carried exclusively by the cell-rich core layer with uniform haematocrit $H = H_b$:

$$\dot{M}_s = \pi(\lambda R)^2 H_b \tag{91}$$

So that Eq. 90 can be expressed finally as:

$$\dot{M}_c = \frac{2D\dot{M}_s}{R^2}\frac{1}{\lambda^2\left(\frac{1}{Sh} - \ln(\lambda)\right)} \tag{92}$$

Here, it is assumed that the local haematocrit $H_b \gg H_c$, as would certainly be true in the case of anaerobic respiration, where the oxygen demand by the cells exceeds the supply, and is compensated for using alternative oxidising-substances found within the cells. It is interesting to observe that the mass transfer then becomes independent of the cell and boundary haematocrits. This expression can be differentiated with respect to λ to obtain:

$$\lambda = \exp\left(\frac{1}{Sh} - \frac{1}{2}\right) \tag{93}$$

Differentiating again with respect to λ shows that this expression represents a local minima in mass transfer, and so seems to suggest that the phase separation does not lead to an optimal mass transfer

rate for any value of λ. Interestingly however, in the case where the diffusion across the vessel membrane were much greater than the intrinsic convection, resulting in $Sh \to \infty$, a minimum in mass transfer would occur at a position of $\lambda = 0.61$, suggesting that this arrangement would in fact be a notable hindrance to diffusion. Similarly, minimising the mass supply needed for a constant cell mass transfer produces the same result.

References

[1] R. Fåhraeus, T. Lindqvist, "The viscosity of the blood in narrow capillary tubes", Am. J. Physiology 96, 562–568 (1931)

[2] A. R. Pries, D. Neuhaus, P. Gaehtgens, "Blood viscosity in tube flow: Dependence on diameter and haematocrit", Am. J. Heart Circ. Physiology 263, H1770-1778 (1992)

[3] G. Segré, A. Silberberg, "Radial particle displacements in Poiseuille flow of suspensions", Nature 189, 209-210 (1961)

[4] B Alberts, A Johnson, J Lewis, "Molecular Biology of the Cell", Garland Science, 2002

[5] C. Uzoigwe, "The human erythrocyte has developed the biconcave disc shape to optimize the flow properties of the blood in the large vessels", Medical Hypothesis 67, 1159–1163 (2006)

[6] W. Reinke, P. Gaehtgens, P. C. Johnson, "Blood viscosity in small tubes: Effect of shear rate, aggregation and sedimentation", Am. J. Heart Circ. Physiology 253, H540-547 (1987)

[7] R.S. Lenk, "Polymer Rheology", Applied Sciences (1978)

[8] W. H. Herschel, R. Bulkley, "Konsistenzmessungen von Gummi-Benzollösungen", Kolloid Zeitschrift 39, 291–300 (1926)

[9] E. W. Merrill, E. R. Gilliland, G. Cokelet, H. Shin, A. Britten, and R. E. Wells Jr., "Rheology of human blood, near and at zero flow: Effects of temperature and haematocrit level", Biophys J. 3.3, 199–213 (1963)

[10] N. Casson, "A flow equation for pigment-oil suspensions of the printing ink type", Rheology of Disperse Systems, 84-104 (1959)

[11] G. Bugliarello, J. Sevilla, "Velocity distribution and other characteristics of steady and pulsatile blood flow in fine glass tubes", Biorheology 7, 85-107 (1970)

[12] A. Einstein, "On the movement of small particles suspended in a stationary liquid demanded by the molecular kinetic theory of heat", Ann. d. Phys. 17, 549-560 (1905)

[13] M. Sharan, A. S. Popel, "A Two-Phase Model for Flow of Blood in Narrow Tubes with Increased Effective Viscosity Near the Wall", Biorheology 38, 415-428 (2001)

[14] S. J. Payne, "A probabilistic approach to two-phase flows in axi-symmetric vessels", personal communication (2012)

[15] C. Chiu, "Entropy and probability concepts in hydraulics", J. Hydraul. Eng. 113(5), 583–599 (1987)

[16] J.R. Womersley, “Method for the calculation of velocity, rate of flow and viscous drag in arteries when the pressure gradient is known”, J. Physiol. 127, 553-563 (1955)

[17] WT McComis, SE Charm, and G Kurland, “Pulsing blood flow in capillary tubes”, Am. J. Physiology 212, 49-53 (1967)

[18] D. Hershey, G. J. Song, “Friction factors and pressure drop for sinusoidal laminar flow of water and blood in rigid tubes”, Am. Inst. Chem. Eng. 43, pages 491–496 (1967)

[19] G. B. Jeffery, “The motion of ellipsoidal particles immersed in a viscous fluid”, Proc. R. Soc. Lond. 102, 161-179 (1922)

[20] Michael A. B. Deakin, ”Erythrocyte distribution in arterial blood flow: The hypothesis of minimal energy dissipation”, Bulletin Math. Biophysics 29, 565-574 (1967)

[21] R. C. Jeffrey, J. R. A. Pearson, ”Particle motion in laminar vertical tube flow”, J. Fluid Mech. 22.4, 721-735 (1965)

[22] J. P. Matas, J. F. Morris, E. Guazzelli, ”Inertial migration of rigid spherical particles in Poiseuille flow”, J. Fluid Mech. 515, 171–195 (2004)

[23] R. V. Repetti, E. F. Leonard, ”Segré-Silberberg annulus formation: A possible explanation”, Nature 203, 1346-1347 (1964)

[24] C. O. Bennett, J. E. Myers “Momentum, Heat, and Mass Transfer”, McGraw-Hill (1962)

[25] A.S. Lubansky, D.V. Boger, ”An approximate solution to flow through a contraction for high Trouton ratio fluids”, J. Non-Newtonian Fluid Mech. 144, 87-97 (2007)

[26] ”Cardano’s formula”, Encyclopedia of Mathematics (2001)

[27] S. I. Rubinow, J. B. Keller, ”The transverse force on a spinning sphere moving in a viscous fluid”, J. Fluid Mech. 11.03, 447-459 (1961)

[28] S. L. Soo, “Pipe flow of suspensions”, Appl. Sci. Res. 21, 68-84 (1969)

[29] H. L. Goldsmith, S. G. Mason, ”The flow of suspensions through tubes: Single spheres, rods and discs”, J. Colloid Science 17, 448-476 (1962)

[30] S. G. Mason, personal communication by Reppetti and Leonard[23]

[31] G. G. Stokes, “On the effect of the internal friction of fluids on the motion of pendulums”, Proc. Cambridge Philos. Soc. 9, 8-106 (1851)